A Bulk Turbulent Air-Sea Flux Algorithm for High-Wind, Spray Conditions

Edgar L Andreas

U.S. Army Cold Regions Research and Engineering Laboratory
Hanover, New Hampshire

Jeffrey E. Hare

P. Ola G. Persson

Corresponding author address: Edgar L Andreas, U.S. Army Cold Regions Research and Engineering Laboratory, 72 Lyme Road, Hanover, NH 03755-1290.
E-Mail: eandreas@crrel.usace.army.mil

November 2006

ABSTRACT

Once the 10-m wind speed over the ocean reaches approximately 12 m s^{-1}, sea spray becomes an important agent for transferring heat and moisture across the air-sea interface. The analysis here establishes that fact by combining the COARE version 2.6 bulk interfacial flux algorithm with a microphysical model to partition measured heat fluxes from two good high-wind data sets into spray and interfacial flux contributions. The measurements come from HEXOS (the experiment to study Heat Exchange over the Sea) and FASTEX (the Fronts and Atlantic Storm-Tracks Experiment); wind speeds in these two data sets span 5 to 20 m s^{-1}.

After separating the measured heat fluxes into spray and interfacial contributions, the manuscript uses the spray fluxes to develop a fast spray flux algorithm to combine with the COARE version 2.6 interfacial flux algorithm in a unified turbulent surface flux algorithm for use in large-scale and ocean storm models. A sensitivity analysis of the spray and interfacial components of this unified flux algorithm demonstrates how the two component fluxes scale differently with the mean meteorological variables and, thus, why they must be parameterized separately in models intended to treat air-sea fluxes in high winds.

1. Introduction

As the surface-level wind speed increases above 10 m s^{-1}, the physics of turbulent air-sea heat transfer changes. In low winds, the turbulent heat transfer occurs almost exclusively at the air-sea interface. But with increasing wind speed, sea spray production increases; and now heat and moisture transfer also occurs at the surface of the spray droplets. We refer to these two ways by which air and sea exchange sensible and latent heat as the interfacial and spray routes.

The fluxes via these two routes scale differently (Andreas 1994; Andreas and DeCosmo 2002). For example, although the COARE version 3.0 bulk flux algorithm (Fairall et al. 2003) has been tuned with flux data collected in wind speeds up to 20 m s^{-1} and is, therefore, operationally useful in this wind speed range, it is based strictly on interfacial scaling and thus may not be reliable if it is extrapolated to wind speed above 20 m s^{-1}. Here, on the other hand, we present a new bulk flux algorithm that explicitly acknowledges the two routes by which heat and moisture cross the air-sea interface. Because we base algorithms for both flux routes on theory and tune the new spray algorithm with data, we expect our algorithm to be reliable on extrapolation to high wind speeds, where flux predictions are essential but validation data do not exist.

We develop our algorithm using data from HEXOS, the experiment on Humidity Exchange over the Sea (Katsaros et al. 1987; Smith et al. 1996; DeCosmo et al. 1996), and FASTEX, the Fronts and Atlantic Storm-Tracks Experiment (Joly et al. 1997; Persson et al. 2005), two of the best available high-wind-speed data sets. Our analysis first uses Andreas's spray microphysics model (Andreas 1989, 1990, 1992) and the COARE version 2.6 interfacial flux algorithm (Fairall et al. 1996) to separate the measured HEXOS and FASTEX sensible and

latent heat fluxes into interfacial and spray contributions. Andreas and DeCosmo (1999, 2002) already demonstrated this partitioning with the HEXOS data.

Next, we fit the resulting spray sensible and latent heat fluxes with parameterizations that allow quick predictions of these fluxes from bulk oceanic and meteorological variables. Our resulting bulk flux algorithm thus comprises the COARE version 2.6 algorithm for the interfacial fluxes and the new algorithm for the spray fluxes. Andreas (2003, 2004) reported preliminary versions of this algorithm.

As a preview of how the interfacial and spray components scale differently, the interfacial fluxes increase almost linearly with the wind speed, while the spray fluxes increase faster than the square of the friction velocity. Likewise, the interfacial sensible heat flux scales with the air-sea temperature difference, while the spray sensible heat flux scales with the difference between the sea surface temperature and the equilibrium temperature of spray droplets that start with a radius of 100 μm; and this latter temperature depends on relative humidity and is almost always lower than the air temperature. Consequently, with no air-sea temperature difference, there is no interfacial sensible heat flux but still, usually, a spray sensible heat flux. Finally, the interfacial latent heat flux scales with the difference between the specific humidity at the ocean surface and at some reference height, while the spray latent heat flux scales with the mass lost by evaporating spray droplets of initial radius 50 μm during their short lifetime between creation and their plunge back into the sea.

2. Spray heat flux model

a. Microphysics

Most of the heat and moisture transfer mediated by spray occurs within a near-surface region that we call the droplet evaporation layer. This layer typically extends about one significant wave height above mean sea level (Andreas et al. 1995; Van Eijk et al. 2001). Spray droplets ejected into this layer start with an initial radius r_0 and the same temperature as the surface seawater, T_s; evolve in both temperature and radius during a brief flight of duration τ_f; and fall back into the sea. This is our conceptual picture of spray-mediated heat and moisture transfer (e.g., Andreas and DeCosmo 1999, 2002).

Under constant environmental conditions, droplet temperature T and radius r evolve as functions of time t approximately as (Andreas 1989, 1990, 2005a; Andreas and DeCosmo 1999, 2002)

$$\frac{T(t) - T_{eq}}{T_s - T_{eq}} = \exp\left(-t/\tau_T\right) \tag{2.1}$$

and

$$\frac{r(t) - r_{eq}}{r_0 - r_{eq}} = \exp\left(-t/\tau_r\right) . \tag{2.2}$$

Here, T_{eq} is the evaporating or equilibrium temperature of a saline droplet with initial radius r_0 and temperature T_s; r_{eq} is the corresponding equilibrium radius of a droplet with initial radius r_0; and τ_T and τ_r are the e-folding times that give the rates for these temperature and radius changes.

Our values for T_{eq}, r_{eq}, τ_T, and τ_r here come from Andreas's (1989, 1990, 1992, 1995) full microphysical spray model, but Andreas (2005a) recently reported algorithms for quickly calculating these four microphysical parameters for use in the flux algorithm that we develop here. Briefly, all four quantities depend on seawater temperature, air temperature (T_a), relative humidity (RH), surface salinity, and initial droplet radius.

Figure 1 shows one example of how spray droplet temperature and radius evolve (cf. Andreas 1990, 1995). With this figure, we also demonstrate two essential points that are fundamental to our sea spray flux algorithm. First, droplet temperature evolves much faster than droplet radius. That is, for all radii and for all environmental conditions, τ_r is typically three orders of magnitude longer than τ_T. Consequently, the spray-mediated sensible and latent heat transfers are decoupled: Evaporation does not really begin until the droplet is sitting at T_{eq}. Secondly, T_{eq} is usually significantly less than the air temperature, and this difference increases with falling relative humidity (cf. Andreas 1995).

Within this microphysical framework, we estimate the temperature of a spray droplet when it falls back into the sea (at time τ_f) as

$$T(\tau_f) = T_{eq} + (T_s - T_{eq})\exp(-\tau_f / \tau_T) \; . \tag{2.3}$$

Consequently, the rate at which all droplets of initial radius r_0 transport sensible heat across the air-sea interface is (Andreas 1992)

$$Q_S(r_0) = \rho_s c_{ps}(T_s - T_{eq})\left[1 - \exp(-\tau_f / \tau_T)\right]\left(\frac{4\pi r_0^3}{3}\frac{dF}{dr_0}\right) \; . \tag{2.4}$$

Here, ρ_s is the density of seawater, and c_{ps} is the specific heat of seawater.

Also in (2.4), dF/dr_0, the spray generation function, is the rate at which droplets of radius r_0 are produced at the sea surface. It has units of number of droplets with radius r_0 produced per square meter of sea surface per second per micrometer increment in droplet radius, $m^{-2}\ s^{-1}\ \mu m^{-1}$. Andreas (2002a) reviews the dF/dr_0 functions available in the literature and recommends the function given by Fairall et al. (1994). Their function is what we use for dF/dr_0 here. In our earlier analysis, Andreas and DeCosmo (2002) had used the Andreas (1992) spray generation function.

Similar arguments lead to an estimate of the latent heat carried by droplets of initial radius r_0. For $\tau_f \le \tau_r$, (2.2) implies that droplets of initial radius r_0 fall back into the sea with radius

$$r(\tau_f) = r_{eq} + (r_0 - r_{eq})\exp(-\tau_f / \tau_r) \ . \tag{2.5}$$

These droplets, therefore, transfer latent heat at the rate

$$Q_L(r_0) = \rho_s L_v \left\{1 - \left[\frac{r(\tau_f)}{r_0}\right]^3\right\}\left(\frac{4\pi r_0^3}{3}\frac{dF}{dr_0}\right) \quad \text{for } \tau_f \le \tau_r \ , \tag{2.6a}$$

where L_v is the latent heat of vaporization.

If the relative humidity is 95% or less, droplets for which $\tau_f > \tau_r$ will have experienced at least two-thirds of their potential moisture loss before they fall back into the sea (Andreas 1992).

For these droplets, we simply assume that $\tau_f >> \tau_r$ and, from (2.5), approximate the rate at which they exchange latent heat as

$$Q_L(r_0) = \rho_s L_v \left[1 - \left(\frac{r_{eq}}{r_0}\right)^3\right]\left(\frac{4\pi r_0^3}{3}\frac{dF}{dr_0}\right) \quad \text{for } \tau_f > \tau_r \ . \tag{2.6b}$$

By integrating $Q_S(r_0)$ and $Q_L(r_0)$ over all radii, we get what Andreas and DeCosmo (1999, 2002) call the "nominal" spray sensible and latent heat fluxes:

$$\overline{Q}_S = \int_{r_1}^{r_2} Q_S(r_0)\,dr_0 \ , \tag{2.7a}$$

$$\overline{Q}_L = \int_{r_1}^{r_2} Q_L(r_0)\,dr_0 \ , \tag{2.7b}$$

where r_1 and r_2 are the smallest and largest droplets that contribute significantly to the integrals. For the Fairall et al. (1994) spray generation function that we use here, $r_1 = 1.6\,\mu m$ and $r_2 = 500\,\mu m$.

Figure 2 shows examples of $Q_S(r_0)$ and $Q_L(r_0)$ for several wind speeds. These quantities have units $W\,m^{-2}\,\mu m^{-1}$. Hence, integrating under these curves over all radii gives the nominal fluxes $\overline{Q}_S$ and $\overline{Q}_L$ in (2.7). Because $\overline{Q}_S$ and $\overline{Q}_L$ are microphysically based, they should have proper theoretical dependence on temperature, humidity, and wind speed. They,

nevertheless, are still "nominal" because of the approximations in (2.4) and (2.6) and, especially, because of the uncertainty in dF/dr_0 (Andreas 2002a).

For estimating the droplet lifetime, τ_f, Andreas (1992) introduced

$$\tau_f = \frac{A_{1/3}}{u_f(r_0)} , \tag{2.8}$$

where $A_{1/3}$ is the significant wave amplitude and $u_f(r_0)$ is the terminal fall speed for droplets of radius r_0 (Friedlander 1977, p. 105; Clift et al. 1978, p. 33ff.; Andreas 1989, 1990). Basically, (2.8) presumes that spume droplets torn right off the wave crests are most important in (2.7).

Lagrangian and Eulerian models of spray droplet dispersion by Edson (Andreas et al. 1995; Edson et al. 1996) and Van Eijk et al. (2001), respectively, support the choice of $A_{1/3}$ as the relevant height scale for the droplet evaporation layer. Mestayer et al. (1996), however, believe that $A_{1/3}$ is too large for this scale; while Kepert et al. (1999) suggest that it is too small.

For $A_{1/3}$ in (2.8), we had been using the traditional expression for the significant wave height based on the Pierson-Moskowitz wave spectrum (e.g., Kinsman 1965, p. 391; Wilson 1965; Earle 1979; Tucker and Pitt 2001, p. 100),

$$H_{1/3} = 0.030\, U_{10}^2 , \tag{2.9}$$

where $H_{1/3}$ (= $2A_{1/3}$) is in meters when U_{10} is the wind speed (in m s^{-1}) at a standard reference height of 10 m. In creating Figure 2, we used (2.9) in (2.8).

But in some of our recent storm modeling (Perrie et al. 2005), we realized that (2.9) was predicting waves that were to high. Hence, on analyzing significant wave heights collected by the U.S. National Data Buoy Center in the northeast Atlantic Ocean, Andreas and Wang (2007) developed an alternative;

$$H_{1/3} = C(D) \quad \text{for } 0 \le U_{10} \le 4\,\mathrm{m\,s^{-1}}\,, \tag{2.10a}$$

$$H_{1/3} = a(D)U_{10}^2 + b(D) \quad \text{for } 4\,\mathrm{m\,s^{-1}} \le U_{10}\,. \tag{2.10b}$$

In these, a(D), b(D), and C(D) are constants that depend on water depth D. Andreas and Wang give these functions. In the bulk flux algorithm that we report here, we replace (2.9) with (2.10).

b. Estimating total heat fluxes

A basic hypothesis in our analysis is that the total sensible ($H_{s,T}$) and latent ($H_{L,T}$) heat fluxes that would be measured, say, with eddy-correlation instruments placed above the droplet evaporation layer are simply linear sums of the interfacial and spray contributions. Taking $\overline{Q}_S$ and $\overline{Q}_L$ from (2.7) as the "nominal" spray fluxes, we formulated this hypothesis as (cf. Fairall et al. 1994; Edson and Andreas 1997; Andreas and DeCosmo 1999, 2002)

$$H_{L,T} = H_L + \alpha \overline{Q}_L\,, \tag{2.11a}$$

$$H_{s,T} = H_s + \beta \overline{Q}_S - (\alpha - \gamma)\overline{Q}_L\,. \tag{2.11b}$$

Here, H_L and H_s are estimates of the interfacial latent and sensible heat fluxes that we compute with our adaptation of the COARE version 2.6 algorithm, which we describe in the appendix. Here also, α, β, and γ are small, non-negative coefficients that we use to tune the nominal spray fluxes to data.

In (2.11a), the α term models the latent heat flux (or the moisture flux) coming out the top of the droplet evaporation layer that spray has contributed. Fairall et al. (1994), however, point out that, because the atmosphere must supply all the heat to evaporate the droplets, these droplets are a sink for sensible heat. Hence, to conserve energy, the α term in (2.11a) must appear with the opposite sign in the sensible heat equation, (2.11b).

The β term in (2.11b) models the sensible heat that spray droplets give up in cooling from the ocean surface temperature T_s to the temperature they have on returning to the sea, $T(\tau_f)$ from (2.3). Some models (e.g., Makin 1998) ignore this term because $\overline{Q}_S$ is typically much smaller than $\overline{Q}_L$ (see Fig. 2), but Andreas and Emanuel (2001) focus on it as the likely route by which spray affects the total air-sea enthalpy flux.

Katsaros and DeCosmo (1990), Smith (1990), Katsaros and de Leeuw (1994), Andreas et al. (1995), and DeCosmo et al. (1996) further speculate that feedbacks within the droplet evaporation layer modify the interfacial fluxes represented by H_s and H_L in (2.11). For example, evaporating droplets cool the droplet evaporation layer and therefore increase the near-surface temperature gradient; the interfacial sensible heat flux would then be larger than the H_s value computed from surface temperature and an air temperature measured above the droplet evaporation layer. We add the γ term in (2.11b) to account for this feedback and expect $\gamma < \alpha$.

A similar process could affect the total latent heat flux. Evaporating spray would moisten the near-surface atmosphere and thereby decrease the near-surface humidity gradient. The actual interfacial latent heat flux would then be smaller than the H_L value computed from the specific humidity measured at the surface and above the droplet evaporation layer. We do not, however, see a way to separate this effect from the spray-mediated flux. Consequently, the α term in (2.11a) possibly includes both the direct spray effect and the humidity feedback effect.

Notice, in light of the above discussion, the total enthalpy flux from the ocean to the atmosphere is the sum of $H_{L,T}$ and $H_{s,T}$,

$$H_{L,T} + H_{s,T} = H_L + H_s + \beta \overline{Q}_S + \gamma \overline{Q}_L \ . \tag{2.12}$$

This flux is the lower boundary conditions in atmospheric models and, for example, is the energy that drives tropical storms (Businger 1982; Emanuel 1995). Notice here that the direct spray latent heat flux, the $\alpha \overline{Q}_L$ term in (2.11a), disappears when we add (2.11a) and (2.11b); only the spray latent heat feedback (the γ term) remains. But the direct spray sensible heat flux, the $\beta \overline{Q}_S$ term, survives the summation and thus is, likely, the main route by which spray affects storm energetics (cf. Andreas and Emanuel 2001).

3. Data

In our earlier work on partitioning interfacial and spray contributions to the sensible and latent heat fluxes, we had used the HEXOS data exclusively (Andreas and DeCosmo 1999, 2002; Andreas 2003, 2004a). DeCosmo (1991), Smith et al. (1992), Katsaros et al. (1994), and DeCosmo et al. (1996) describe this data set and the instruments used to obtain it. Briefly, the HEXOS data were collected in the North Sea from the Meetpost Noordwijk platform, where the water is only 18 m deep. The HEXOS set contains 175 runs in which the turbulent fluxes of momentum and sensible and latent heat were measured by eddy correlation in 10-m winds up to 18.3 m s^{-1}. Many of the runs include two measurements of the latent heat flux—one using a Lyman-α hygrometer, and the other using wet and dry thermocouples. Each run also includes measurements of the significant wave height. Andreas and DeCosmo (2002) describe some preprocessing that we had to do on DeCosmo's (1991) tabulated data to obtain the variables we require.

Here, we add the FASTEX turbulent flux data (Persson et al. 2005) to our analysis. These data came from a mast placed on the bow of the *R/V Knorr* as the ship crossed the North Atlantic from England to Nova Scotia at latitudes between 52°N and 40°N from 23 December 1996 to 26 January 1997. The FASTEX set includes 322 hourly measurements of the momentum and sensible and latent heat fluxes by eddy correlation and simultaneous measurements of the significant wave height.

Besides the turbulent fluxes, both the HEXOS and FASTEX sets include accompanying measurements of mean meteorological quantities—like wind speed, air and sea surface temperature, and humidity. In our flux partitioning, which is based on (2.11), we assume $H_{L,T}$ and $H_{s,T}$ are the reported HEXOS and FASTEX sensible and latent heat fluxes. We compute

"nominal" fluxes, $\overline{Q}_L$ and $\overline{Q}_S$, from the microphysical model described in Section 2a and these mean meteorological quantities. We also use the mean meteorological quantities in the flux algorithm described in the appendix to compute the interfacial fluxes in (2.11), H_L and H_s.

In analyzing the FASTEX data, we used the interfacial algorithm as it is described in the appendix. Because the HEXOS site was in only 18 m of water, however, (A5) is not the best parameterization for predicting the roughness length z_0. Therefore, for the HEXOS analysis, we estimated z_0 from the drag relation found specifically for the HEXOS site (Smith et al. 1992; cf. Andreas and DeCosmo 2002),

$$C_{DN10} = \left(0.27 + 0.116\, U_{N10}\right)\times 10^{-3} \ . \tag{3.1}$$

Here, C_{DN10} is the neutral-stability drag coefficient at a reference height of 10 m, and U_{N10} is the neutral-stability wind speed (in m s^{-1}) at 10 m. The HEXOS data set includes U_{N10}. With (3.1), our estimate of the roughness length for the HEXOS analysis is

$$z_0 = 10 \exp\left(-k\, C_{DN10}^{-1/2}\right) \ , \tag{3.2}$$

which gives z_0 in meters. All other aspects of our HEXOS analysis were as described in the appendix.

The surface salinity affects the four microphysical constants T_{eq}, r_{eq}, τ_T, and τ_r. We also included salinity effects when we calculated the surface specific humidity, Q_s in (A1c). For the HEXOS site, we used a surface salinity of 34 psu; for the FASTEX transect, we used a typical value of 36 psu.

4. Separating spray and interfacial fluxes

a. Without spray

To justify our focus on spray effects, we first state the null hypothesis: *The HEXOS and FASTEX heat flux data are well represented by an interfacial flux algorithm* . If this hypothesis were true, a state-of-the-art bulk flux algorithm that parameterizes only interfacial heat transfer should be able to reproduce both data sets. COARE version 2.6 is such an algorithm: It is based on a theory that recognizes only interfacial transfer (i.e., Liu et al. 1979) and is well validated for wind speeds up to 10 m s^{-1} where, we believe, interfacial transfer dominates (e.g., Fairall et al. 1996; Grant and Hignett 1998; Chang and Grossman 1999).

Figure 3, however, shows the results when we model the HEXOS and FASTEX sets with the interfacial flux algorithm described in the appendix. That is, we invoke (2.11) but exclude spray effects by setting $\alpha = \beta = \gamma = 0$. Figure 3 depicts the ratio of the measured flux ($H_{L,T}$ or $H_{s,T}$) to the modeled flux (H_L or H_s in this case) as a function of U_{N10}. Call these ratios R_L and R_S, respectively, for latent and sensible heat flux.

If COARE 2.6 were adequate for explaining the HEXOS and FASTEX heat fluxes, the measured/modeled ratios would average one, and the ratios would show no dependence on wind speed—that is, the correlation coefficients in Fig. 3 would be zero. But both panels in Fig. 3 fail both tests: COARE 2.6 explains neither the magnitude nor the wind speed dependence of the combined HEXOS/FASTEX set. To put these conclusions on firm statistical footing, we test whether the averages of the ratios in Fig. 3 are statistically different from one and whether the correlation coefficients are statistically different from zero.

Any elementary statistics text explains that, if the sample size N is large enough,

$$\mu - \frac{z_{\alpha/2}\, s}{\sqrt{N}} \le \bar{x} \le \mu + \frac{z_{\alpha/2}\, s}{\sqrt{N}} \tag{4.1}$$

is a $(1 - \alpha)$% confidence interval for the sample mean $\bar{x}$. Here also, s is the sample standard deviation, and $z_{\alpha/2}$ is the $(1 - \alpha/2)100$ percentage point of a Normal distribution. In our case, we test the hypothesis that $\mu = 1.00$; and let's test at the 1% significance level (so $\alpha = 0.01$ and $z_{\alpha/2} = 2.576$).

For the latent heat flux panel in Fig. 3 (where N = 486), the 99% confidence interval on the average of R_L, from (4.1), is $[0.965,1.035]$. For the sensible heat flux panel (where N = 337), the 99% confidence interval for the average of R_S is $[0.944,1.056]$. From the values listed in the caption for Fig. 3, we see that both latent and sensible heat flux average ratios are far outside these 99% confidence intervals. We thus establish statistically that an algorithm that includes only interfacial transfer cannot explain the magnitude of the HEXOS and FASTEX heat fluxes.

Likewise, Bendat and Piersol (1971, p. 126f.) describe the distribution for the sample correlation coefficient r_{xy} between two variables x and y. Briefly, if the sample is large enough, the statistic

$$\bar{w} = \frac{1}{2} \ln\left(\frac{1 + r_{xy}}{1 - r_{xy}}\right) \tag{4.2}$$

has a Normal distribution with mean

$$\mu_w = \frac{1}{2}\ln\left(\frac{1+\rho_{xy}}{1-\rho_{xy}}\right) \tag{4.3}$$

and variance

$$\sigma_w^2 = \frac{1}{N-3} \ . \tag{4.4}$$

In (4.3), ρ_{xy} is the true correlation coefficient. With this formalism, a $(1-\alpha)100\%$ confidence interval for $\overline{w}$ is

$$-z_{\alpha/2} \le \frac{\overline{w}-\mu_w}{\sigma_w} \le z_{\alpha/2} \ . \tag{4.5}$$

Because we are testing the hypothesis that $\rho_{xy} = 0$, $\mu_w = 0$ from (4.3). We further rearrange (4.5) to obtain the following $(1-\alpha)100\%$ confidence interval for r_{xy},

$$\frac{\exp\left(-2z_{\alpha/2}\sigma_w\right)-1}{\exp\left(-2z_{\alpha/2}\sigma_w\right)+1} \le r_{xy} \le \frac{\exp\left(2z_{\alpha/2}\sigma_w\right)-1}{\exp\left(2z_{\alpha/2}\sigma_w\right)+1} \ . \tag{4.6}$$

Again, testing at the 1% significance level, we calculate the 99% confidence interval for the correlation coefficient in the latent heat flux panel in Fig. 3 to be $[-0.117, 0.117]$; for the sensible heat flux panel, $[-0.140, 0.140]$. Because the correlation coefficients mentioned in the

caption for Fig. 3 are far outside these intervals, we confirm that an algorithm that models only interfacial transfer cannot explain the wind speed behavior of the combined HEXOS/FASTEX data set. We thus reject the null hypothesis that an interfacial flux algorithm is adequate for explaining turbulent heat flux data collected in high winds.

b. With spray

When faced with a dilemma similar to that presented in Fig. 3—the heat flux measurements were larger than the model predictions at high wind speeds—Fairall et al. (2003; their Fig. 4) assumed the model parameterizations for z_T and z_Q [see (A2b) and (A2c)] were inadequate. They, thus, tuned new z_T and z_Q parameterizations to their data and continued assuming implicitly that the turbulent heat fluxes were strictly through interfacial processes all the way up to wind speeds of 20 m s^{-1}.

While this is a reasonable operational approach, our earlier work—both theoretical and data-based—suggests that the spray route is significant for air-sea heat transfer when the 10-m wind speed reaches 12–15 m s^{-1} (Andreas 1992; Andreas et al. 1995; Andreas and DeCosmo 2002). The fact that both R_S and R_L increase in Fig. 3 with wind speed is compatible with the argument that spray-mediated transfer is augmenting the interfacial transfer.

Of course, some unrecognized process, instead of spray, may be enhancing the heat fluxes; but in (2.11), we have a theoretical model with which to account for spray transfer. If this model can explain the HEXOS and FASTEX fluxes, we may not need to look for other transfer processes.

Accounting for spray effects starts with evaluating α in (2.11a). Again, we presume that the nominal spray latent heat flux, $\overline{Q}_L$, is approximately correct; α should then be of order one.

We tune it with the HEXOS and FASTEX data and have two methods for judging the best α value. As we saw with Fig. 3, we want the average of the R_L ratios to be near one and the correlation coefficient of R_L with U_{N10} to be near zero. Figure 4 shows these two metrics as α increases from 0 to 5.

In Fig. 4, the correlation coefficient is zero and the least-squares fitting line is, thus, horizontal for $\alpha = 1.5$. The figure also shows that, there, the average of the R_L ratios is 1.03, which, according to the discussion in the last subsection, is not statistically different from 1.00. Hence, we adopt $\alpha = 1.5$.

Evaluating β and γ in (2.11b) is not as straightforward, however. Again, we want to obtain an average value for the ratio of measured-to-modeled sensible heat flux (i.e., average of R_S) near one and a correlation coefficient between R_S and U_{N10} near zero. By varying β and γ over a range of plausible values, we settled on $\beta = 10.5$ and $\gamma = 0.2$.

This combination produces an average value for R_S of 0.98 and an R_S-U_{N10} correlation coefficient of 0.083. The statistical tests described in the last subsetion confirm that this R_S average is not statistically different from 1.00 and that the correlation coefficient is not statistically different from 0.00. We thus adopt $\beta = 10.5$ and $\gamma = 0.2$ for use in (2.11b).

Viewed in the context of the enthalpy flux, (2.12), this small γ value tends to confirm Andreas and Emanuel's (2001) conclusion that the spray sensible heat flux is the primary route by which spray effects storm energy. The spray latent heat flux appears in (2.12) only as the small feedback term $\gamma \overline{Q}_L$ that arises because the evaporating spray cools the near-surface air and, thereby, enhances the air-sea temperature difference.

Figure 5 is like Fig. 3 but in it, instead, we include spray effects in the modeled heat fluxes through (2.11) and the α, β, and γ values that we have just found. In the latent heat flux

panel, the least squares line is horizontal—that is, the R_L values have no wind speed dependence. In the sensible heat flux panel, the least squares line has a slight positive slope that is not statistically different from zero. In each panel, the average of the plotted points is not statistically different from 1.00.

Figure 5 also highlights cases with at least a 10% spray contribution. That is, in the latent heat flux panel, filled markers denote cases for which $\left|\alpha \overline{Q}_L / H_L\right| \geq 0.1$; in the sensible heat flux panel, filled markers denote $\left|\left[\beta \overline{Q}_S - (\alpha - \gamma)\overline{Q}_L\right] / H_s\right| \geq 0.1$. In the latent heat flux panel, most cases with $U_{N10} > 13$ m s^{-1} include at least a 10% spray effect. In the sensible heat flux panel, almost all cases for which $U_{N10} > 11$ m s^{-1} include at least a 10% spray effect.

To recap, we first showed that a state-of-the-art bulk flux algorithm that treats only interfacial fluxes can explain neither the magnitude nor the wind speed dependence of the combined HEXOS/FASTEX heat fluxes. But by complementing this interfacial flux algorithm with a theoretically based model that explicitly accounts for spray-mediated transfer, we have explained both the magnitude and the wind speed dependence of the HEXOS/FASTEX set. This analysis also let us separate the measured fluxes into interfacial and spray contributions and thereby established that spray-mediated fluxes become significant (at least a 10% effect) in this data set when the 10-m wind speed reaches 11–13 m s^{-1}.

5. Spray flux algorithm

The microphysical model that produced the spray fluxes $\overline{Q}_S$ and $\overline{Q}_L$ in (2.11) is too complex and too computer intensive for use in large-scale models. One of our purposes here, then, is to develop a fast spray flux algorithm comparable in speed to the COARE version 2.6 algorithm that we use to compute H_s and H_L in (2.11). The flux partitioning that went into our producing Fig. 5 is the basis for this new spray flux algorithm.

Equation (2.4) suggests that the sensible heat flux carried by all droplets of initial radius r_0 scales with $\rho_s\, c_{ps}\left(T_s - T_{eq}\right)$ since the droplet residence time τ_f is usually much longer than the temperature evolution time τ_T. Furthermore, Fig. 2 shows that droplets with initial radii near 100 μm contribute most to $\overline{Q}_S$. Hence, as a simple model, we assume that these 100-μm droplets are the bellwethers of the spray sensible heat flux and, thus, model it as

$$Q_{S,sp} \equiv \beta \overline{Q}_S - (\alpha - \gamma)\overline{Q}_L = \rho_s\, c_{ps}\left(T_s - T_{eq,100}\right) V_s\left(u_*\right) . \tag{5.1}$$

Here, $Q_{S,sp}$ is in W m^{-2}; $T_{eq,100}$ is the equilibrium temperature of these 100-μm droplets; and $V_S(u_*)$ is a wind function that we parameterize in terms of the friction velocity and evaluate from the spray sensible heat fluxes that we found in the last section.

Figure 6 shows

$$V_S\left(u_*\right) \equiv \frac{\beta \overline{Q}_S - (\alpha - \gamma)\overline{Q}_L}{\rho_s\, c_{ps}\left(T_s - T_{eq,100}\right)} \tag{5.2}$$

for the combined HEXOS/FASTEX set, where we computed $T_{eq,100}$ from Andreas's (2005a) fast microphysical algorithm. The data follow a power law relation fairly well and, thus, confirm that (5.1) is a reasonable parameterization for the spray sensible heat flux. We obtain

$$V_s(u_*) = 2.30\times10^{-6}\, u_*^3 \ , \tag{5.3}$$

where V_S is in m s^{-1} for u_* in m s^{-1}. In Fig. 6, almost all cases for which u_* is greater than 0.4 m s^{-1} display at least a 10% spray effect in the sensible heat flux.

We follow similar reasoning to obtain a parameterization for the spray latent heat flux. Equation (2.6a) implies that the spray latent heat flux mediated by all droplets of initial radius r_0 scales as $\rho_s L_v \left\{1 - \left[r(\tau_f)/r_0 \right]^3 \right\}$. Moreover, Fig. 2 shows that droplets with initial radii near 50 μm contribute most to $\overline{Q}_L$. As a simple parameterization, we therefore hypothesize that these 50-μm droplets are good indicators of the total spray latent heat flux and model it as

$$Q_{L,sp} \equiv \alpha \overline{Q}_L = \rho_s L_v \left\{1 - \left[\frac{r(\tau_{f,50})}{50\,\mu m} \right]^3 \right\} V_L(u_*) \ . \tag{5.4}$$

Here, $Q_{L,sp}$ is in W m^{-2}; $\tau_{f,50}$ is the approximate residence time for droplets with 50-μm initial radius, which we compute from (2.8); $r(\tau_{f,50})$ is the radius these droplets have when they fall back into the sea [see (2.5)]; and the 50 μm reiterates our hypothesis that 50-μm droplets lead the spray latent heat flux.

Equation (5.4) introduces another wind function, V_L, which we define as

$$V_L(u_*) \equiv \frac{\alpha \overline{Q}_L}{\rho_s L_v \left\{1 - \left[r\left(\tau_{f,50}\right)/50\,\mu\text{m} \right]^3 \right\}} \ . \tag{5.5}$$

Figure 7 shows how we evaluated this function from the HEXOS and FASTEX data. To obtain $r(\tau_{f,50})$ in (5.5), we used Andreas's (2005a) fast microphysical algorithms to compute $r_{eq,50}$ and $\tau_{r,50}$ in (2.5); these are, respectively, the equilibrium radius of a droplet that starts with a radius of 50 μm and the time scale for reaching that equilibrium radius.

As with V_S, V_L follows a power law in u_*. Our result is

$$V_L(u_*) = 1.10\times10^{-7}\, u_*^{2.22} \ , \tag{5.6}$$

which gives V_L in m s^{-1} when u_* is in m s^{-1}. In Fig. 7, most cases for which u_* is greater than 0.6 m s^{-1} include at least a 10% spray effect in the latent heat flux.

In summary, our spray flux algorithm for high-wind, spray conditions converts from (2.11) to

$$H_{L,T} = H_L + Q_{L,sp} \ , \tag{5.7a}$$

$$H_{s,T} = H_s + Q_{S,sp} \ . \tag{5.7b}$$

In this, the interfacial fluxes H_L and H_s come, basically, from the COARE version 2.6 algorithm, as described in the appendix. The spray-mediated sensible heat flux, $Q_{S,sp}$, comes from (5.1) and (5.3); the spray-mediated latent heat flux, $Q_{L,sp}$, comes from (5.4), (5.6), (2.5), and (2.8). The approximations reported in Andreas (2005a) provide the necessary microphysical variables $T_{eq,100}$, $r_{eq,50}$, and $\tau_{r,50}$.

As typical in bulk flux algorithms, we solve for H_s and H_L iteratively. After the solution converges, we use the resulting value of u_* to compute V_S and V_L from (5.3) and (5.5). That is, as yet, the interfacial and spray fluxes are uncoupled. We identify the algorithm we describe here as version 3.1 of our bulk spray flux algorithm. That algorithm also includes a parameterization that Andreas (2004b) reports for how spray alters the near-surface stress profile. Andreas (2003, 2004a), Andreas and Emanuel (2001), and Perrie et al. (2005) have described earlier versions of this algorithm.

6. Sensitivity studies

To highlight how the interfacial and spray contributions to the total air-sea heat and moisture fluxes scale differently, we show in Figs. 8–10 some sensitivity calculations based on our bulk flux algorithm. Andreas (2004a) and Perrie et al. (2005) show similar sensitivity plots based on earlier versions of our flux algorithm.

Figure 8 shows H_s, H_L, $Q_{S,sp}$, and $Q_{L,sp}$ as functions of wind speed for fixed relative humidity and air and surface temperatures. Realized we are making these calculations for wind speeds well beyond the range for which our flux parameterizations have been tested. But because both the interfacial and spray flux parameterizations are theoretically based, we have some justification for these extrapolations. In fact, the theoretical basis for the heat flux parameterization in the COARE version 2.6 algorithm (i.e., Liu et al. 1979)—as opposed to the operational basis in COARE version 3.0 (Fairall et al. 2003)—is the reason we use it in our algorithm.

The interfacial sensible and latent heat fluxes in Fig. 8 increase almost linearly with wind speed. The spray heat fluxes, on the other hand, are small for 10-m wind speeds less than about 12 m s^{-1} but then increase faster than the square of the wind speed because of (5.3) and (5.6). Because $Q_{S,sp}$ and $Q_{L,sp}$ are small and increase approximately linearly with wind speed for speeds less than 20 m s^{-1}, the COARE version 3.0 algorithm can be operationally successful by using interfacial scaling to parameterize the total latent and sensible heat fluxes in this wind speed range. But extrapolating that algorithm to winds speeds above 20 m s^{-1} is not appropriate because the nonlinear dependencies of $Q_{S,sp}$ and $Q_{L,sp}$ on wind become significant.

Figure 9 shows a similar flux plot, but here the surface temperature varies from 0° to 30°C with U_{10} fixed at 25 m s^{-1}. Again, this plot shows how the interfacial and spray fluxes

scale differently. The interfacial latent heat flux, H_L, increases at a faster rate than linear with surface temperature because both Q_s and Q_r in (A1c) are exponential functions of temperature. In contrast, the spray latent heat flux, $Q_{L,sp}$, increases nearly linearly with T_s because $r_{eq,50}$ in (2.5) does not depend strongly on temperature (Andreas 2005a) while $\tau_{r,50}$, which does, is compared with and comparable to $\tau_{f,50}$ (Andreas 1992; Andreas and DeCosmo 1999).

The interfacial and spray sensible heat fluxes in Fig. 9 are both approximately linear in surface temperature; but H_s decreases slightly with increasing T_s, while $Q_{S,sp}$ increases slightly. The decrease in H_s is basically because the air density decreases with increasing temperature. The increase in $Q_{S,sp}$ results because $T_s - T_{eq,100}$ [see (5.1)] increases with increasing temperature (Andreas 1995) faster than the product $\rho_s c_{ps}$ decreases (Andreas 2005b). Hence, again, because H_s and $Q_{S,sp}$ scale differently, over extended ranges in parameter space, it is not wise to parameterize the total sensible heat flux using interfacial scaling.

Figure 10 is the last sensitivity plot. This shows how the fluxes depend on relative humidity for the range of relative humidities over which our microphysical model is valid, 75–100% . In the figure, both the interfacial and spray latent heat fluxes decrease with relative humidity. The interfacial flux, H_L, is essentially linear in relative humidity and stays positive through the range of humidities because T_a is always 2°C less than T_s [see (A1c)]. $Q_{L,sp}$, in contrast, is not linear in relative humidity and actually goes negative when the relative humidity is above about 98% because the salinity (34 psu) depresses the saturation vapor pressure over spray droplets. That is, at these high relative humidities, vapor can condense on the spray droplets.

Also in Fig. 10, the interfacial sensible heat flux is essentially independent of relative humidity. If the winds were much weaker, H_s could depend weakly on relative humidity through

stratification effects. For a wind speed of 25 m s^{-1}, however, the surface layer stratification is nearly neutral. The spray sensible heat flux, $Q_{S,sp}$, does decrease with increasing relative humidity, however. This behavior results because $T_{eq,100}$ [see (5.1)] gets closer and closer to the air temperature, T_a, as the relative humidity increased toward 98% (Andreas 1995).

In summary, Fig. 10 reiterates that using interfacial scaling over an extended parameter space in which spray can make significant contributions to the heat fluxes is not appropriate. Treating the interfacial and spray fluxes separately, as we do in (2.11) and (5.7), is a more sound approach.

7. Conclusions

Theoretical studies (Andreas 1992, 1998; Andreas et al. 1995) and our earlier analysis of the flux data from HEXOS (Andreas and DeCosmo 1999, 2002) suggest that spray-mediated fluxes can account for at least 10% of the air-sea sensible and latent heat fluxes once the 10-m wind speed exceeds about 12 m s^{-1}. Still, most current bulk air-sea flux algorithms acknowledge only the interfacial contributions to the air-sea sensible and latent heat fluxes (e.g., Fairall et al. 1996, 2003; Zeng et al. 1998; Bourassa et al. 1999). Such algorithms cannot be reliably extrapolated to storm winds because the spray and interfacial fluxes scale differently with wind speed and other meteorological variables. Nevertheless, some models developed especially for ocean storms have tried to incorporate spray effects with mixed results (Fairall et al. 1994; Kepert et al. 1999; Bao et al. 2000; Andreas and Emanuel 2001; Wang et al. 2001; Perrie et al. 2004, 2005). But of these storm models, only those by Andreas and Emanuel (2001) and Perrie et al. (2004, 2005) have spray parameterizations actually tuned with data because they derive from our earlier analysis of the HEXOS data.

In light of the need for a quick, reliable spray parameterization, to our previous HEXOS analysis, we have thus added the much larger set of air-sea flux measurements from FASTEX, another very good high-wind data set. Applying microphysical theory and our knowledge of the spray generation function, we identify a spray signature in the combined HEXOS/FASTEX set. As Andreas and DeCosmo (2002) did, we apply multiple tests to confirm these spray effects. First, we showed that a state-of-the-art bulk flux algorithm—COARE version 2.6—that parameterizes only interfacial transfer can explain neither the magnitude nor the wind speed dependence of either the measured sensible or latent heat fluxes in the combined HEXOS/FASTEX set.

But, next, by adding a spray flux parameterization to the interfacial flux algorithm, we could explain both the magnitude and the wind speed dependence of the sensible and latent heat fluxes in our data set. As we had seen earlier, our current analysis revealed at least a 10% spray effect on the total sensible and latent heat fluxes at fairly modest wind speeds: for 10-m wind speeds above about 11 m s^{-1} for the sensible heat flux, and for winds above about 13 m s^{-1} for the latent heat flux.

Because we based these calculations on a full microphysical model that is too time consuming for large-scale or operational storm modeling, we developed a much simpler bulk spray flux algorithm from our partitioning the heat fluxes into spray and interfacial contributions. For the spray sensible heat flux, we based this algorithm on the behavior of droplets that started with radius 100 μm since these seem to lead the spray sensible heat transfer (see Fig. 2). We likewise based the algorithm for the spray latent heat transfer on the behavior of droplets that were originally 50 μm in radius. These droplets are near the peak in the radius-specific spray latent heat flux (see Fig. 2).

The key to this spray flux algorithm was evaluating the so-called wind functions V_S and V_L shown in (5.2) and (5.5) and in Figs. 6 and 7. Both of these functions increase faster than the square of the friction velocity u_*—a result that emphasizes why spray-mediated heat transfer becomes increasingly important in storm winds.

Examples of sensitivity calculations in Figs. 8–10 that are based on this new flux algorithm demonstrate further how the interfacial and spray fluxes scale differently. We intend with these figures to underscore the hazards of using interfacial scaling to parameterize heat fluxes measured in winds, nominally, above 11–13 m s^{-1}. If the data were collected over limited ranges in humidity and in air and surface temperatures, the analysis may look good. But

extrapolating these results outside the ranges they represent could produce unreliable results because of differences in how the interfacial and spray fluxes scale.

We have developed FORTRAN code for our combined spray and interfacial bulk flux algorithm and are willing to share it. We want to close with one important caveat, though. Our spray flux algorithm is intimately tied to the COARE version 2.6 interfacial flux algorithm because, essentially, we obtained the spray fluxes that we used to develop the spray flux algorithm by subtracting COARE version 2.6 predictions of the interfacial fluxes from the measured HEXOS and FASTEX heat fluxes. This approach is the only way we have found to separate the spray and interfacial fluxes. Therefore, if you use equations for the spray flux algorithm that we give here or if you extract just the spray flux algorithm from our FORTRAN code and combine it with your favorite bulk interfacial flux algorithm, you will be misusing our results. To use our spray flux algorithm to compute the spray-mediated fluxes, you must also use the COARE version 2.6 interfacial flux algorithm to compute the interfacial fluxes if you ultimately want the total air-sea sensible and latent heat fluxes.

Acknowledgements. The Office of Naval Research supported this work with award N0001406MP20089. We thank Bill Otto for providing the FASTEX wave heights and Chris Fairall for several useful discussions about this work.

APPENDIX

Interfacial Flux Algorithm

We base our calculations of the interfacial sensible (H_s) and latent (H_L) heat fluxes and the momentum flux (τ) on the COARE version 2.6 algorithm (Fairall et al. 1996). We prefer this version of the COARE algorithm to the more recent version (3.0; Fairall et al. 2003) because predictions for the roughness lengths for temperature (z_T) and humidity (z_Q) in version 2.6 are based on the surface renewal theory of Liu et al. (1979) and are validated with data for wind speeds up to about 10 m s^{-1} (Fairall et al. 1996), where spray should have a negligible effect on the turbulent heat fluxes.

For version 3.0, on the other hand, Fairall et al. (2003) obtained empirical expression for z_T and z_Q using flux data collected in winds up to 20 m s^{-1}, where we suspect spray contributions are significant. Since Fairall et al. use interfacial scaling throughout this wind speed range, their expressions for z_T and z_Q likely include entangled spray and interfacial effects. Since these two contributions do not scale the same, we do not believe the version 3.0 z_T and z_Q predictions will be reliable when extrapolated to wind speeds above 20 m s^{-1}.

The COARE algorithm is based on Monin-Obukhov similarity theory. The three interfacial fluxes are calculated as

$$\tau \equiv \rho_a u_*^2 = \rho_a C_{Dr} S_r^2 , \tag{A1a}$$

$$H_s = \rho_a c_p C_{Hr} S_r \left(\Theta_s - \Theta_r\right) , \tag{A1b}$$

$$H_L = \rho_a L_v C_{Er} S_r \left(Q_s - Q_r\right) . \tag{A1c}$$

Here, (A1a) defines the friction velocity u_*; S_r, Θ_r, and Q_r are the effective wind speed, potential temperature, and specific humidity at reference height r; Θ_s (= T_s) is the potential temperature at the water surface; and Q_s is the specific humidity at the surface. Also in (A1), ρ_a is the air density; c_p, the specific humidity of air at constant pressure; and L_v, the latent heat of vaporization.

Monin-Obukhov similarity theory enters by providing a theoretical basis for specifying the transfer coefficients for momentum (C_{Dr}), sensible heat (C_{Hr}), and latent heat (C_{Er}) appropriate at height r;

$$C_{Dr} = \frac{k^2}{\left[\ln\left(r/z_0\right) - \psi_m\left(r/L\right)\right]^2} , \qquad \text{(A2a)}$$

$$C_{Hr} = \frac{k^2}{\left[\ln\left(r/z_0\right) - \psi_m\left(r/L\right)\right]\left[\ln\left(r/z_T\right) - \psi_h\left(r/L\right)\right]} , \qquad \text{(A2b)}$$

$$C_{Er} = \frac{k^2}{\left[\ln\left(r/z_0\right) - \psi_m\left(r/L\right)\right]\left[\ln\left(r/z_Q\right) - \psi_h\left(r/L\right)\right]} . \qquad \text{(A2c)}$$

Here, k (= 0.40) is the von Kármán constant; z_0 is the roughness length for wind speed; z_T and z_Q are the roughness lengths for temperature and humidity that we have already discussed; and ψ_m and ψ_h are empirical stratification corrections that are functions of r/L, where L is the Obukhov length. Equations (A1) and (A2) must be solved iteratively because they are coupled through L.

We invoke the gustiness parameterization in the COARE algorithm to estimate the effective wind speed (S_r) in unstable stratification from the reported wind speed (U_r),

$$S_r = \left(U_r^2 + \beta_g^2 w_*^2\right)^{1/2} . \quad \text{(A3)}$$

Here, $\beta_g = 1.25$, and w_* is Deardorff's (1970) convective velocity scale (Godfrey and Beljaars 1991). For stable stratification, we adopt the suggestion by Jordan et al. (1999) that a similar "windless" coefficient is necessary but express it as

$$S_r = U_r + 0.5\,\mathrm{sech}\left(U_r\right) . \quad \text{(A4)}$$

This gives S_r in m s^{-1} when U_r is in m s^{-1}. Equation (A4) prevents a singularity when U_r is near zero (cf. Zeng et al. 1998), but S_r and U_r are essentially the same when U_r is $5\,\mathrm{m\,s^{-1}}$ or greater.

For z_0 in (A2), the COARE algorithm (Fairall et al. 1996, 2003) uses a smooth blending between aerodynamically smooth flow and a Charnock relation (e.g., Zilitinkevich 1969; Smith 1988),

$$z_0 = 0.135\frac{\nu}{u_*} + 0.0185\frac{u_*^2}{g} . \quad \text{(A5)}$$

Here, z_0 is in meters when u_* is in m s^{-1}; ν, the kinematic viscosity of air, is in m^2 s^{-1}; and g, the acceleration of gravity, is in m s^{-2}. The COARE algorithm uses a coefficient of 0.11 in the first

term on the right of (A3), but 0.135 agrees better with the known behavior of the flow speed profile in aerodynamically smooth flow (Andreas et al. 2006).

The COARE version 2.6 algorithm uses 0.011 for the coefficient of the second term on the right in (A5). But for version 3.0, Fairall et al. (2003) allow that coefficient to increase linearly from 0.011 to 0.018 as the 10-m wind speed increases from 10 to 18 m s^{-1}. We just use a constant value of 0.0185 for this coefficient, though, because this value is appropriate for the high winds speeds and young waves that are our focus (Wu 1982; Johnson et al. 1998).

Our interfacial flux algorithm differs from the COARE algorithms in other small ways. For ψ_m and ψ_h in (A2), we use Paulson's (1970) functions in unstable stratification and Holtslag and De Bruin's (1988) in stable stratification, as recommended by Jordan et al. (1999) and Andreas (2002b). Since our focus is on high wind speeds, these functions will yield insignificantly different results from the COARE algorithm's functions (Fairall et al. 1996, 2003). We also do not incorporate the cool-skin and warm-layer parameterizations that are hallmarks of the COARE algorithm under the assumption that, for the high winds that characterize our data set, the true water surface temperature, T_s, is within the measurement uncertainty of the near-surface bulk water temperature.

Finally, we do not allow values of the scalar roughness lengths z_T and z_Q, computed from the Liu et al. (1979) theory, to be smaller than the mean free path of air molecules, nominally 7×10^{-8} m (cf. Andreas and Emanuel 2001). Both z_T and z_Q fall to this level when u_* exceeds 0.88 m s^{-1}, approximately. Hence, this limit affected only one HEXOS run and only a few FASTEX runs.

REFERENCES

Andreas, E. L, 1989: Thermal and size evolution of sea spray droplets. CRREL Rep. 89-11, U.S. Army Cold Regions Research and Engineering Laboratory, Hanover, NH, 37 pp. [NTIS: ADA210484.]

_____, 1990: Time constants for the evolution of sea spray droplets. *Tellus*, **42B**, 481–497.

_____, 1992: Sea spray and the turbulent air-sea heat fluxes. *J. Geophys. Res.*, **97**, 11,429–11,441.

_____, 1994: Reply. *J. Geophys. Res.*, **99**, 14,345–14,350.

_____, 1995: The temperature of evaporating sea spray droplets. *J. Atmos. Sci.*, **52**, 852–862.

_____, 1998: A new sea spray generation function for wind speeds up to 32 m s^{-1}. *J. Phys. Oceanogr.*, **28**, 2175–2184.

_____, 2002a: A review of the sea spray generation function for the open ocean. *Atmosphere-Ocean Interactions*, Vol. 1, W. Perrie, Ed., WIT Press, 1–46.

_____, 2002b: Parameterizing scalar transfer over snow and ice: A review. *J. Hydrometeor.*, **3**, 417–432.

_____, 2003: An algorithm to predict the turbulent air-sea fluxes in high-wind, spray conditions. Preprints, *12th Conf. on Interaction of the Sea and Atmosphere*, Long Beach, CA, Amer. Meteor. Soc., CD-ROM 3.4, 7 pp.

_____, 2004a: A bulk air-sea flux algorithm for high-wind, spray conditions, Version 2.0. Preprints, *13th Conference on Interactions of the Sea and Atmosphere*, Portland, ME, Amer. Meteor. Soc., CD-ROM P1.5, 8 pp.

_____, 2004b: Spray stress revisited. *J. Phys. Oceanogr.*, **34**, 1429–1440.

_____, 2005a: Approximation formulas for the microphysical properties of saline droplets. *Atmos. Res.*, **75**, 323–345.

_____, 2005b: Handbook of physical constants and functions for use in atmospheric boundary layer studies. ERDC/CRREL Monograph M-05-1, U.S. Army Cold Regions Research and Engineering Laboratory, Hanover, NH, 42 pp.

_____, and J. DeCosmo, 1999: Sea spray production and influence on air-sea heat and moisture fluxes over the open ocean. *Air-Sea Exchange: Physics, Chemistry and Dynamics*, G. L. Geernaert, Ed., Kluwer, 327–362.

_____, and _____, 2002: The signature of sea spray in the HEXOS turbulent heat flux data. *Bound.-Layer Meteor.*, **103**, 303–333.

_____, and K. A. Emanuel, 2001: Effects of sea spray on tropical cyclone intensity. *J. Atmos. Sci.*, **58**, 3741–3751.

_____, and S. Wang, 2007: Predicting significant wave height off the northeast coast of the United States. *Ocean Engng.*, to appear.

_____, J. B. Edson, E. C. Monahan, M. P. Rouault, and S. D. Smith, 1995: The spray contribution to net evaporation from the sea: A review of recent progress. *Bound.-Layer Meteor.*, **72**, 3–52.

_____, K. J. Claffey, R. E. Jordan, C. W. Fairall, P. S. Guest, P. O. G. Persson, and A. A. Grachev, 2006: Evaluations of the von Kármán constant in the atmospheric surface layer. *J. Fluid Mech.*, **559**, 117–149.

Bao, J.-W., J. M. Wilczak, J.-K. Choi, and L. H. Kantha, 2000: Numerical simulations of air-sea interaction under high wind conditions using a coupled model: A study of hurricane development. *Mon. Wea. Rev.*, **128**, 2190–2210.

Bendat, J. S., and A. G. Piersol, 1971: *Random Data: Analysis and Measurement Procedures*. Wiley-Interscience, 407 pp.

Bourassa, M. A., D. G. Vincent, and W. L. Wood, 1999: A flux parameterization including the effects of capillary waves and sea state. *J. Atmos. Sci.*, **56**, 1123–1139.

Businger, J. A., 1982: The fluxes of specific enthalpy, sensible heat and latent heat near the Earth's surface. *J. Atmos. Sci.*, **39**, 1889–1892.

Chang, H.-R., and R. L. Grossman, 1999: Evaluation of bulk surface flux algorithms for light wind conditions using data from the Coupled Ocean-Atmosphere Response Experiment (COARE). *Quart. J. Roy. Meteor. Soc.*, **125**, 1551–1588.

Clift, R., J. R. Grace, and M. E. Weber, 1978: *Bubbles, Drops, and Particles*. Academic Press, 380 pp.

Deardorff, J. W., 1970: Convective velocity and temperature scales for the unstable planetary boundary layer and for Rayleigh convection. *J. Atmos. Sci.*, **27**, 1211–1213.

DeCosmo, J., 1991: Air-sea exchange of momentum, heat and water vapor over whitecap sea states. Ph.D. dissertation, University of Washington, 212 pp.

_____, K. B. Katsaros, S. D. Smith, R. J. Anderson, W. A. Oost, K. Bumke, and H. Chadwick, 1996: Air-sea exchange of water vapor and sensible heat: The Humidity Exchange over the Sea (HEXOS) results. *J. Geophys. Res.*, **101**, 12,001–12,016.

Earle, M. D., 1979: Practical determinations of design wave conditions. *Ocean Wave Climate*, M. D. Earle and A. Malahoff, Eds., Plenum Presss, 39–60.

Edson, J. B., and E. L Andreas, 1997: Modeling the role of sea spray on air-sea heat and moisture exchange. Preprints, *12th Symp. on Boundary Layers and Turbulence*, Vancouver, British Columbia, Amer. Meteor. Soc., 490–491.

_____, S. Anquentin, P. G. Mestayer, and J. F. Sini, 1996: Spray droplet modeling: 2. An interactive Eulerian-Lagrangian model of evaporating spray droplets. *J. Geophys. Res.*, **101**, 1279–1293.

Emanuel, K. A., 1995: Sensitivity of tropical cyclones to surface exchange coefficients and a revised steady-state model incorporating eye dynamics. *J. Atmos. Sci.*, **52**, 3969–3976.

Fairall, C. W., J. D. Kepert, and G. J. Holland, 1994: The effect of sea spray on surface energy transports over the ocean. *Global Atmos. Ocean System*, **2**, 121–142.

_____, E. F. Bradley, D. P. Rogers, J. B. Edson, and G. S. Young, 1996: Bulk parameterization of air-sea fluxes for Tropical Ocean-Global Atmosphere Coupled-Ocean Atmosphere Response Experiment. *J. Geophys. Res.*, **101**, 3747–3764.

_____, _____, J. E. Hare, A. A. Grachev, and J. B. Edson, 2003: Bulk parameterization of air-sea fluxes: Updates and verification for the COARE algorithm. *J. Climate*, **16**, 571–591.

Friedlander, S. K., 1977: *Smoke, Dust and Haze: Fundamentals of Aerosol Behavior*. John Wiley & Sons, 317 pp.

Godfrey, J. S., and A. C. M. Beljaars, 1991: On the turbulent fluxes of buoyancy, heat and moisture at the air-sea interface at low wind speeds. *J. Geophys. Res.*, **96**, 22,043–22,048.

Grant, A. L. M., and P. Hignett, 1998: Aircraft observations of the surface energy balance in TOGA-COARE. *Quart. J. Roy. Meteor. Soc.*, **124**, 101–122.

Holtslag, A. A. M., and H. A. R. De Bruin, 1988: Applied modeling of the nighttime surface energy balance over land. *J. Appl. Meteor.*, **27**, 689–704.

Johnson, H. K., J. Højstrup, H. J. Vested, and S. E. Larsen, 1998: On the dependence of sea surface roughness on wind waves. *J. Phys. Oceanogr.*, **28**, 1702–1716.

Joly, A., and 19 others, 1997: The Fronts and Atlantic Storm-Track Experiment (FASTEX): Scientific objectives and experimental design. *Bull. Amer. Meteor. Soc.*, **78**, 1917–1940.

Jordan, R. E., E. L Andreas, and A. P. Makshtas, 1999: Heat budget of snow-covered sea ice at North Pole 4. *J. Geophys. Res.*, **104**, 7785–7806.

Katsaros, K. B., and J. DeCosmo, 1990: Evaporation in high wind speeds, sea surface temperature at low wind speeds, examples of atmospheric regulation. Preprints, *Modelling the Fate and Influence of Marine Spray*, P. G. Mestayer, E. C. Monahan, and P. A. Beetham, Eds., Marine Sciences Institute, University of Connecticut, Groton, 106–114.

_____, and G. de Leeuw, 1994: Comment on "Sea spray and the turbulent air-sea heat fluxes" by Edgar L Andreas. *J. Geophys. Res.*, **99**, 14,339–14,343.

_____, S. D. Smith, and W. A. Oost, 1987: HEXOS—Humidity Exchange over the Sea, a program for research on water-vapor and droplet fluxes from sea to air at moderate to high wind speeds. *Bull. Amer. Meteor. Soc.*, **68**, 466–476.

_____, J. DeCosmo, R. J. Lind, R. J. Anderson, S. D. Smith, R. Krann, W. Oost, K. Uhlig, P. G. Mestayer, S. E. Larsen, M. H. Smith, and G. de Leeuw, 1994: Measurements of humidity and temperature in the marine environment during the HEXOS Main Experiment. *J. Atmos. Oceanic Technol.*, **11**, 964–981.

Kepert, J., C. Fairall, and J.-W. Bao, 1999: Modelling the interaction between the atmospheric boundary layer and evaporating sea spray droplets. *Air-Sea Exchange: Physics, Chemistry and Dynamics*, G. L. Geernaert, Ed., Kluwer, 363–409.

Kinsman, B., 1965: *Wind Waves*. Prentice-Hall, 676 pp.

Liu, W. T., K. B. Katsaros, and J. A. Businger, 1979: Bulk parameterization of air-sea exchanges of heat and water vapor including the molecular constraints at the interface. *J. Atmos. Sci.*, **36**, 1722–1735.

Makin, V. K., 1998: Air-sea exchange of heat in the presence of wind waves and spray. *J. Geophys. Res.*, **103**, 1137–1152.

Mestayer, P. G., A. M. J. Van Eijk, G. de Leeuw, and B. Tranchant, 1996: Numerical simulation of the dynamics of sea spray over the waves. *J. Geophys. Res.*, **101**, 20,771–20,797.

Paulson, C. A., 1970: The mathematical representation of wind speed and temperature profiles in the unstable atmospheric surface layer. *J. Appl. Meteor.*, **9**, 857–861.

Perrie, W., X. Ren, W. Zhang, and Z. Long, 2004: Simulation of extratropical Hurricane Gustav using a coupled atmosphere-ocean-sea spray model. *Geophys. Res. Lett.*, **31** (L03110), 4 pp. (doi: 10.1029/2003GL018571.)

_____, E. L Andreas, W. Zhang, W. Li, J. Gyakum, and R. McTaggart-Cowan, 2005: Sea spray impacts on intensifying midlatitude cyclones. *J. Atmos. Sci.*, **62**, 1867–1883.

Persson, P. O. G., J. E. Hare, C. W. Fairall, and W. D. Otto, 2005: Air-sea interaction processes in warm and cold sectors of extratropical cyclonic storms observed during FASTEX. *Quart. J. Roy. Meteor. Soc.*, **131**, 877–912.

Smith, S. D., 1988: Coefficients for sea surface wind stress, heat flux, and wind profiles as a function of wind speed and temperature. *J. Geophys. Res.*, **93**, 15,467–15,472.

_____, 1990: Influence of droplet evaporation on HEXOS humidity and temperature profiles. Preprints, *Modelling the Fate and Influence of Marine Spray*, P. G. Mestayer, E. C. Monahan, and P. A. Beetham, Eds., Marine Sciences Institute, University of Connecticut, Groton, 171–174.

_____, R. J. Anderson, W. A. Oost, C. Krann, N. Maat, J. DeCosmo, K. B. Katsaros, K. L. Davidson, K. Bumke, L. Hasse, and H. Chadwick, 1992: Sea surface wind stress and drag coefficients: The HEXOS results. *Bound.-Layer Meteor.*, **60**, 109–142.

_____, K. B. Katsaros, W. A. Oost, and P. G. Mestayer, 1996: The impact of the HEXOS programme. *Bound.-Layer Meteor.*, **78**, 121–141.

Tucker, M. J., and E. G. Pitt, 2001: *Waves in Ocean Engineering*. Elsevier, 521 pp.

Van Eijk, A. M. J., B. S. Tranchant, and P. G. Mestayer, 2001: SeaCluse: Numerical simulation of evaporating sea spray droplets. *J. Geophys. Res.*, **106**, 2573–2588.

Wang, Y., J. D. Kepert, and G. J. Holland, 2001: The effect of sea spray evaporation on tropical cyclone boundary layer structure and intensity. *Mon. Wea. Rev.* **129**, 2481–2500.

Wilson, B. W., 1965: Numerical prediction of ocean waves in the North Atlantic for December, 1959. *Dtsch. Hydrogr. Z.*, **18**, 114–130.

Wu, J., 1982: Wind-stress coefficients over sea surface from breeze to hurricane. *J. Geophys. Res.*, **87**, 9704–9706.

Zeng, X., M. Zhao, and R. E. Dickinson, 1998: Intercomparison of bulk aerodynamic algorithms for the computation of sea surface fluxes using TOGA COARE and TAO data. *J. Climate*, **11**, 2628–2644.

Zilitinkevich, S. S., 1969: On the computation of the basic parameters of the interaction between the atmosphere and the ocean. *Tellus*, **21**, 17–24.

CAPTIONS OF FIGURES

Fig. 1. Temperature and radius evolution of a spray droplet with initial radius 100 μm (r_0), initial temperature 20°C (T_s), and initial salinity 34 psu. This droplet is flung into air with temperature 18°C (T_a) and relative humidity 90% (RH); the barometric pressure is 1000 mb. The microphysical quantities T_{eq}, r_{eq}, τ_T, and τ_r characterize the evolution [see (2.1) and (2.2)].

Fig. 2. The radius-specific spray sensible (Q_S) and latent (Q_L) heat fluxes [from (2.4) and (2.6)] as functions of the radius at formation (r_0) for three values of the wind speed at a 10-m reference height (U_{10}). For these calculations, the water temperature (T_s) is 20°C, the air temperature (T_a) is 18°C, the relative humidity (RH) is 90%, the barometric pressure is 1000 mb, and the surface salinity is 34 psu.

Fig. 3. Ratios of HEXOS and FASTEX measurements of the latent and sensible heat fluxes and the corresponding fluxes modeled with a strictly interfacial flux algorithm (i.e., COARE 2.6; see appendix). U_{N10} is the neutral-stability wind speed at 10 m. The dashed line in each panel represents the best fit to the data. In the latent heat flux plot, the ratio average is 1.094 and the correlation coefficient is 0.176; in the sensible heat flux plot, the average is 1.124, and the correlation coefficient is 0.274.

Fig. 4. Evaluating α in (2.11a) from the combined HEXOS and FASTEX set of measured latent heat fluxes. The left vertical axis is the average of measured-to-modeled values of the latent heat flux (i.e., the average of R_L); the right axis is the correlation coefficient between R_L and U_{N10}. The correct α value produces an average near one and a correlation coefficient near zero.

Fig. 5. As in Fig. 3, except here we include spray in the modeled heat fluxes through (2.11) with $\alpha = 1.5$, $\beta = 10.5$, and $\gamma = 0.2$. In the latent heat flux panel, the average of the plotted ratios is 1.031, and the R_L-U_{N10} correlation coefficient is 0.000; in the sensible heat flux panel, the average of the ratios is 0.980, and the R_S-U_{N10} correlation coefficient is 0.072. The filled markers denote cases for which the modeled spray contribution [the α, β, and γ terms in (2.11)] sum to at least 10% of the corresponding modeled interfacial contribution (the H_s and H_L terms).

Fig. 6. The wind function V_S defined by (5.2) and obtained from the HEXOS and FASTEX data. As in Fig. 5, the filled markers denote cases with at least a 10% spray effect. The line is (5.3).

Fig. 7. The wind function V_L defined by (5.5) and obtained from the HEXOS and FASTEX data. As in Fig. 5, the filled markers denote cases with at least a 10% spray effect. The line is (5.6).

Fig. 8. Calculations made with the bulk flux algorithm described here of the interfacial (H_s and H_L) and spray ($Q_{S,sp}$ and $Q_{L,sp}$) fluxes as functions of the 10-m wind speed, U_{10}. Air temperature is fixed at 18°C, surface temperature is 20°C, relative humidity is 90%, sea surface salinity is 34 psu, and barometric pressure is 1000 mb.

Fig. 9. As in Fig. 8, except here the fluxes are plotted against surface temperature for the wind speed fixed at 25 m s^{-1}. Again, the relative humidity is 90%, but the air temperature is always 2°C less than the surface temperature.

Fig. 10. As in Fig. 8, except here the fluxes are plotted against relative humidity for the wind speed fixed at 25 m s^{-1}.

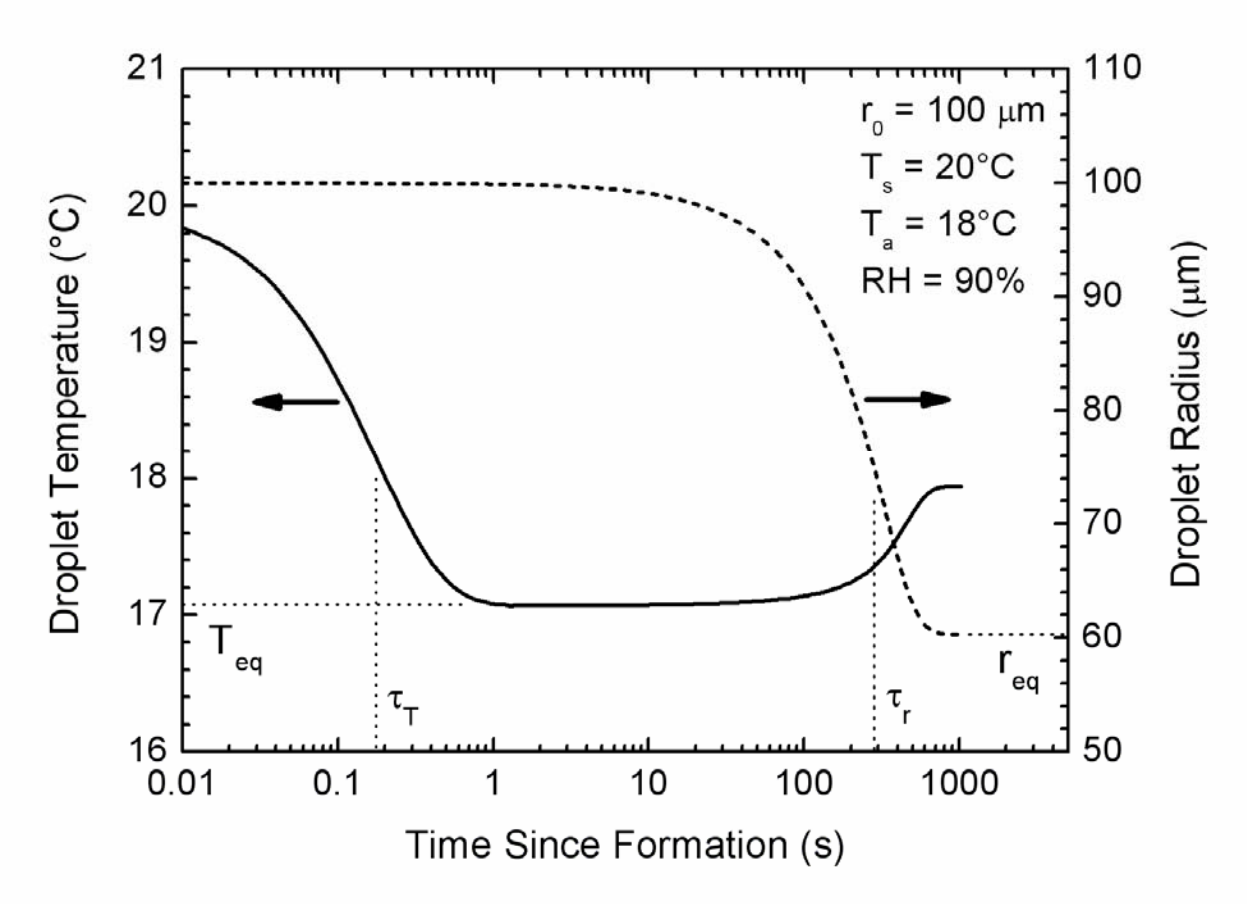

Fig. 1. Temperature and radius evolution of a spray droplet with initial radius 100 μm (r_0), initial temperature 20°C (T_s), and initial salinity 34 psu. This droplet is flung into air with temperature 18°C (T_a) and relative humidity 90% (RH); the barometric pressure is 1000 mb. The microphysical quantities T_{eq}, r_{eq}, τ_T, and τ_r characterize the evolution [see (2.1) and (2.2)].

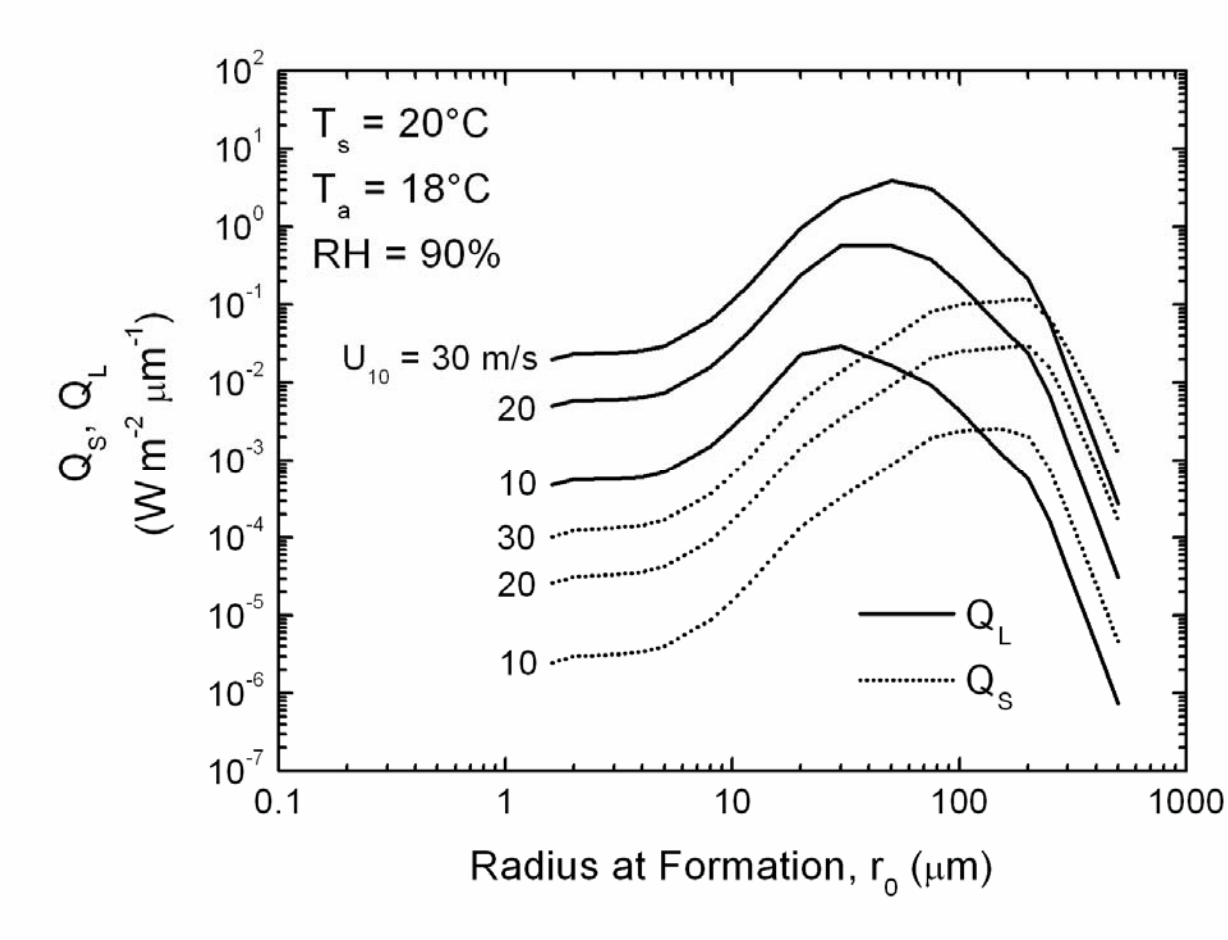

Fig. 2. The radius-specific spray sensible (Q_S) and latent (Q_L) heat fluxes [from (2.4) and (2.6)] as functions of the radius at formation (r_0) for three values of the wind speed at a 10-m reference height (U_{10}). For these calculations, the water temperature (T_s) is 20°C, the air temperature (T_a) is 18°C, the relative humidity (RH) is 90%, the barometric pressure is 1000 mb, and the surface salinity is 34 psu.

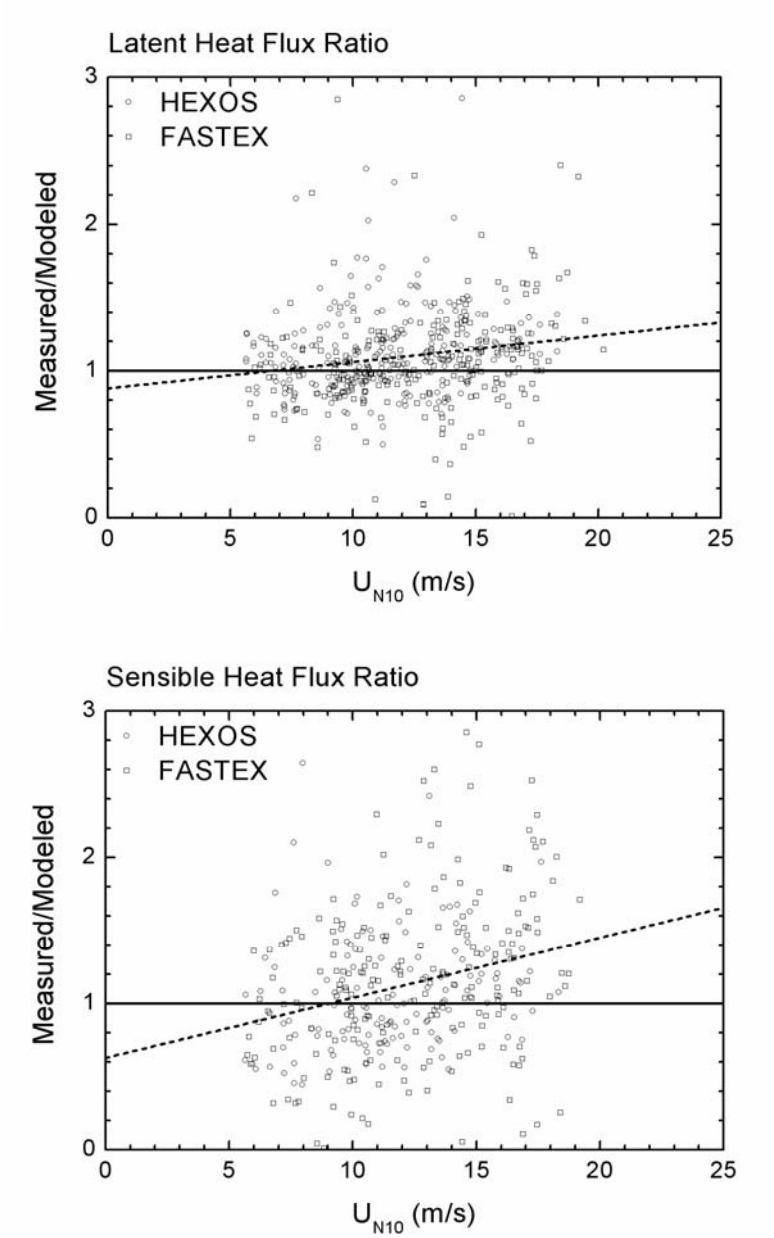

Fig. 3. Ratios of HEXOS and FASTEX measurements of the latent and sensible heat fluxes and the corresponding fluxes modeled with a strictly interfacial flux algorithm (i.e., COARE 2.6; see appendix). U_{N10} is the neutral-stability wind speed at 10 m. The dashed line in each panel represents the best fit to the data. In the latent heat flux plot, the ratio average is 1.094 and the correlation coefficient is 0.176; in the sensible heat flux plot, the average is 1.124, and the correlation coefficient is 0.274.

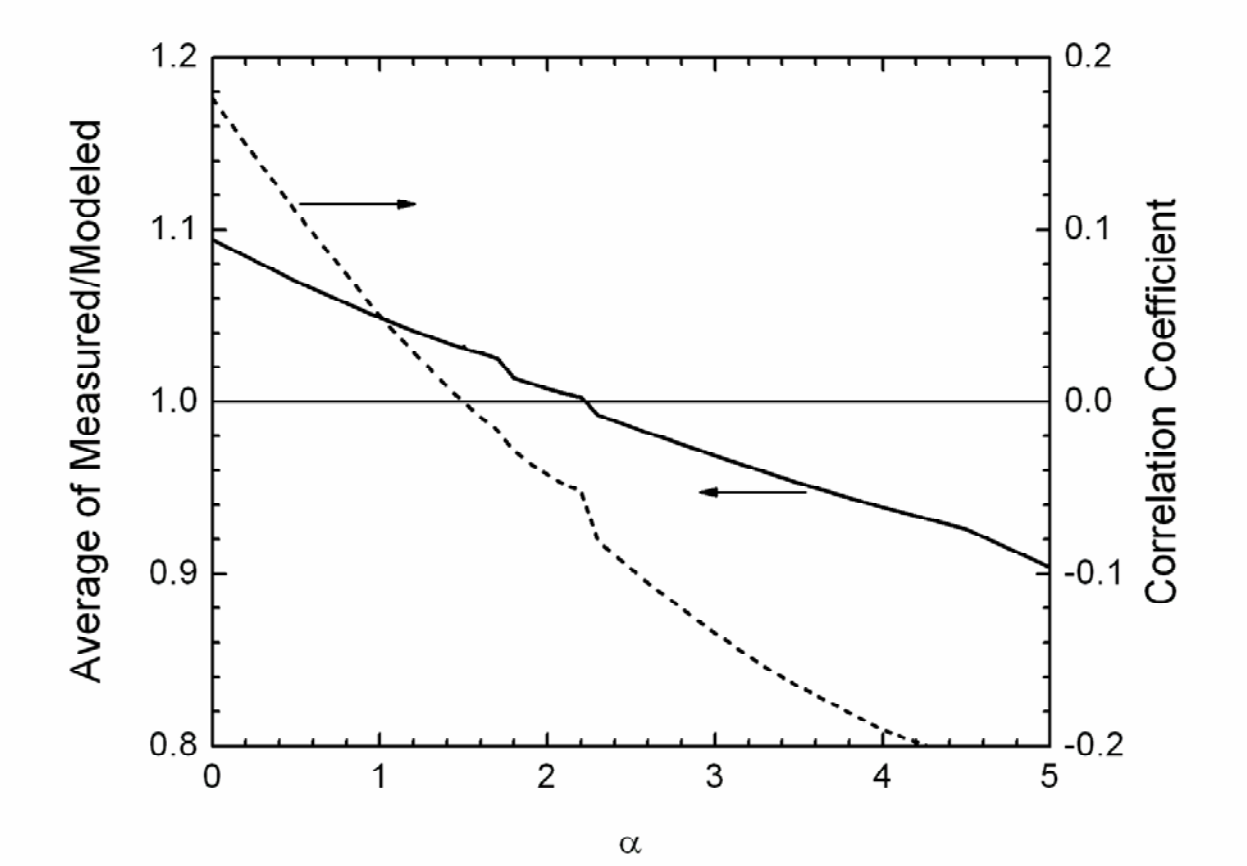

Fig. 4. Evaluating α in (2.11a) from the combined HEXOS and FASTEX set of measured latent heat fluxes. The left vertical axis is the average of measured-to-modeled values of the latent heat flux (i.e., the average of R_L); the right axis is the correlation coefficient between R_L and U_{N10}. The correct α value produces an average near one and a correlation coefficient near zero.

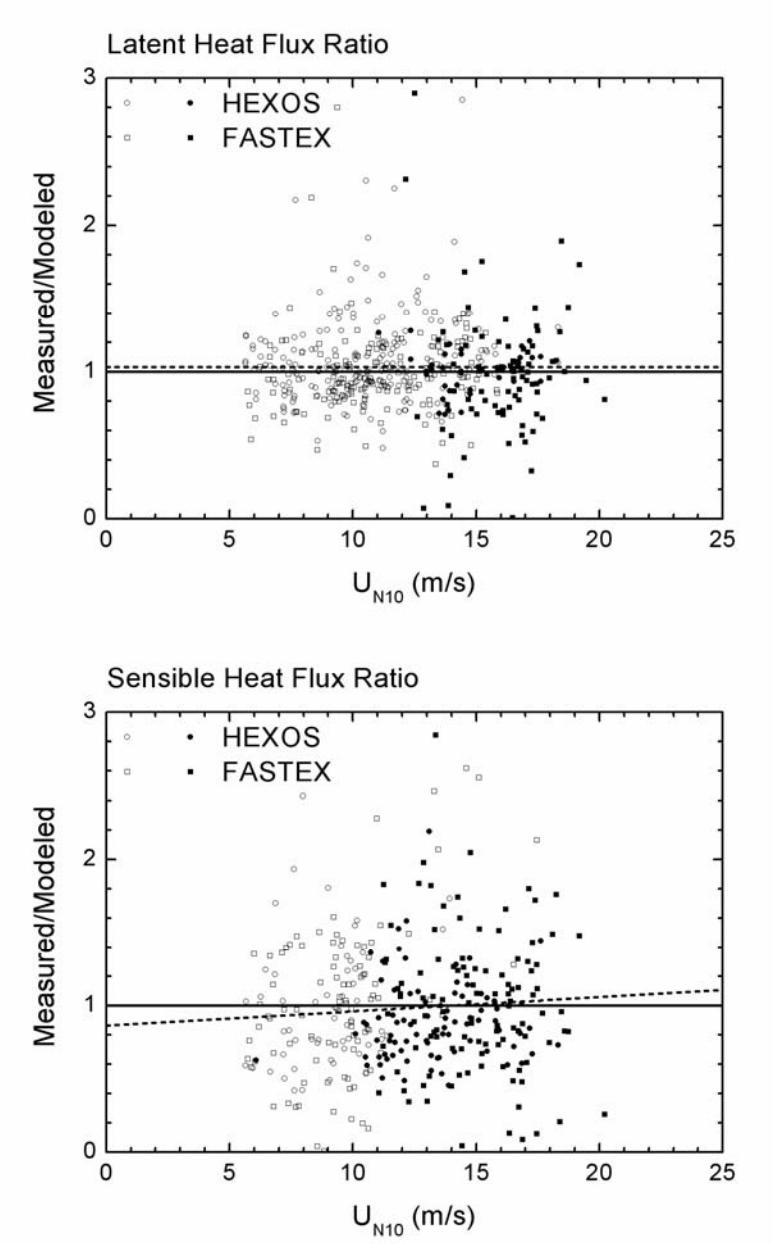

Fig. 5. As in Fig. 3, except here we include spray in the modeled heat fluxes through (2.11) with $\alpha = 1.5$, $\beta = 10.5$, and $\gamma = 0.2$. In the latent heat flux panel, the average of the plotted ratios is 1.031, and the R_L-U_{N10} correlation coefficient is 0.000; in the sensible heat flux panel, the average of the ratios is 0.980, and the R_S-U_{N10} correlation coefficient is 0.072. The filled markers denote cases for which the modeled spray contribution [the α, β, and γ terms in (2.11)] sum to at least 10% of the corresponding modeled interfacial contribution (the H_s and H_L terms).

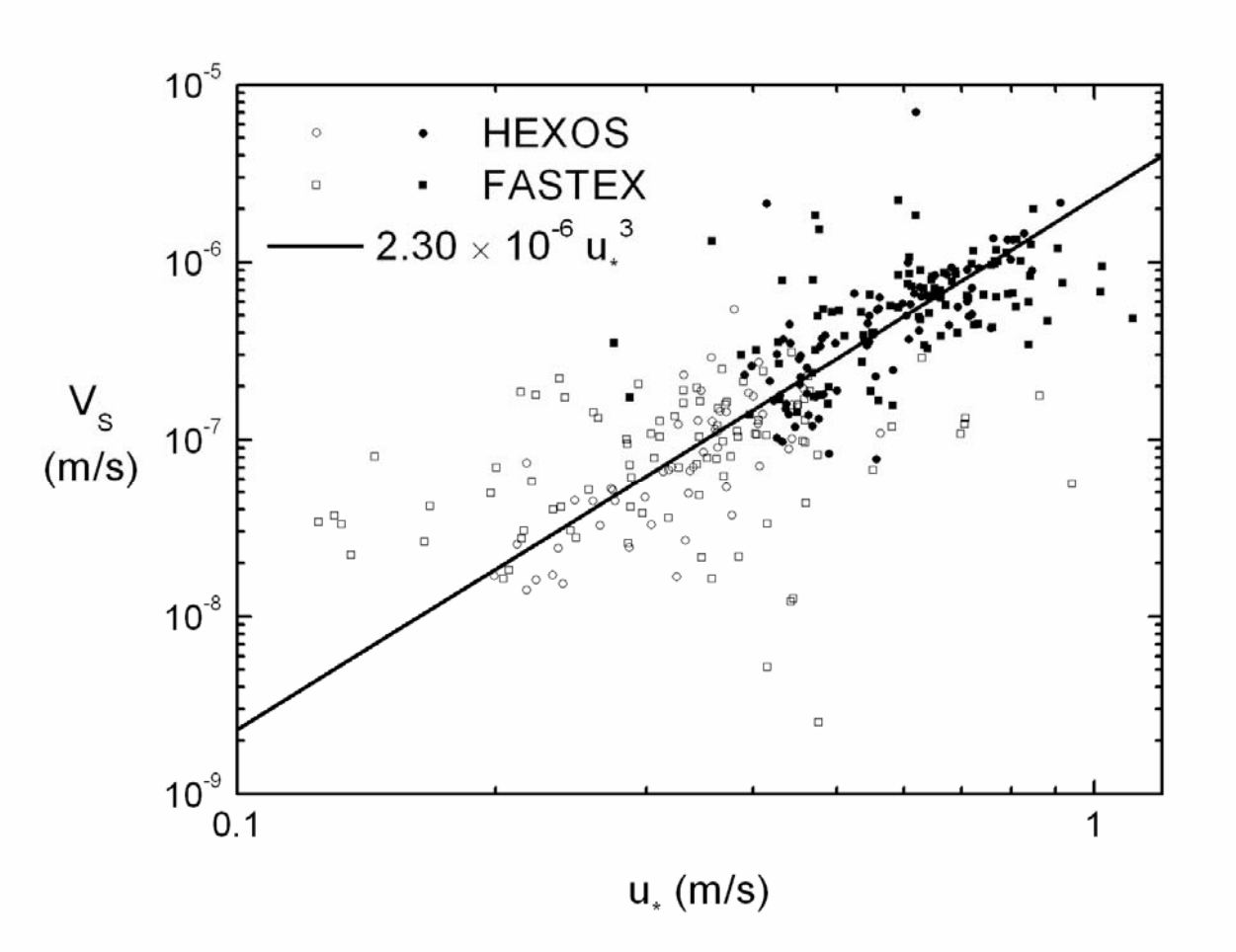

Fig. 6. The wind function V_S defined by (5.2) and obtained from the HEXOS and FASTEX data. As in Fig. 5, the filled markers denote cases with at least a 10% spray effect. The line is (5.3).

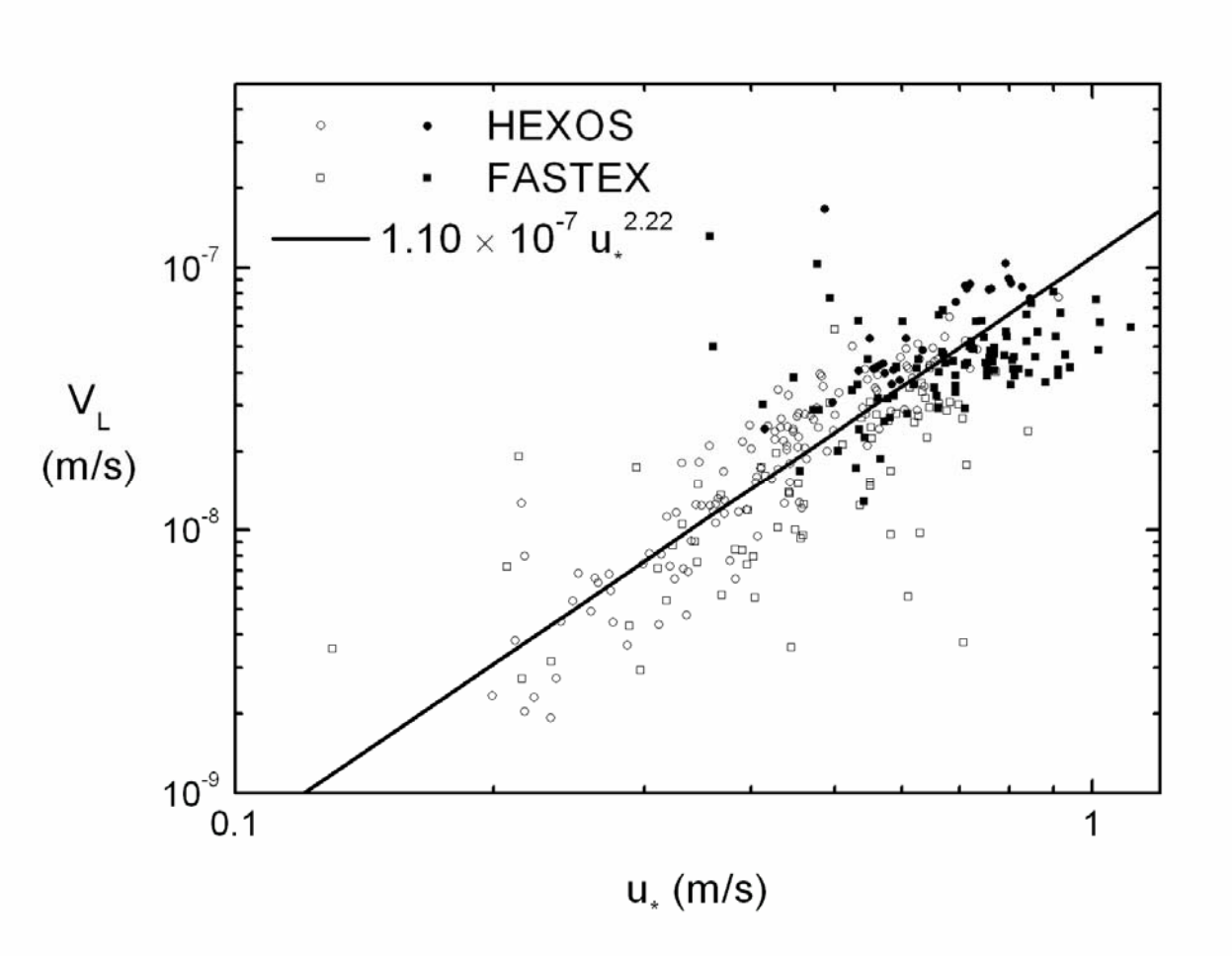

Fig. 7. The wind function V_L defined by (5.5) and obtained from the HEXOS and FASTEX data. As in Fig. 5, the filled markers denote cases with at least a 10% spray effect. The line is (5.6).

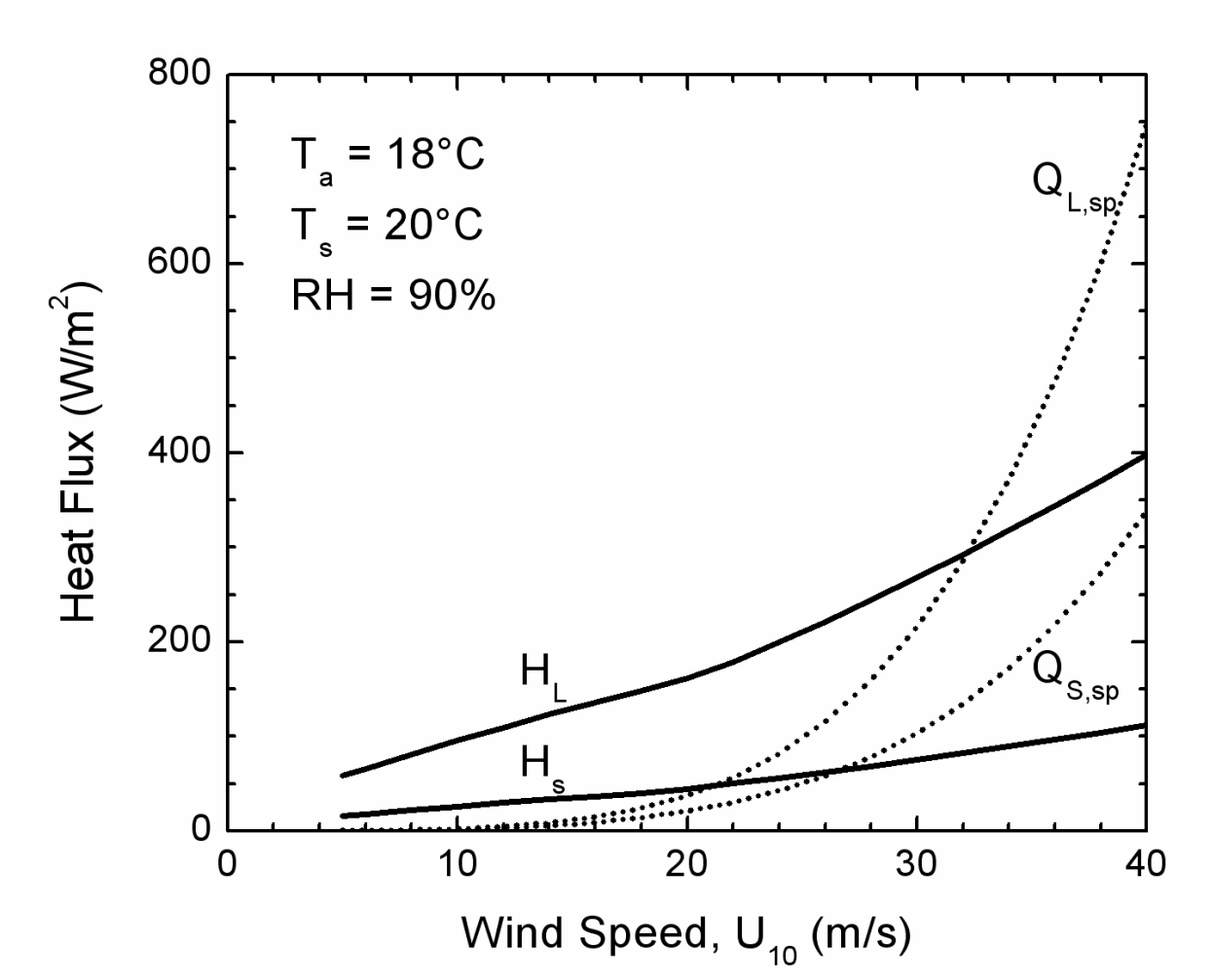

Fig. 8. Calculations made with the bulk flux algorithm described here of the interfacial (H_s and H_L) and spray ($Q_{S,sp}$ and $Q_{L,sp}$) fluxes as functions of the 10-m wind speed, U_{10}. Air temperature is fixed at 18°C, surface temperature is 20°C, relative humidity is 90%, sea surface salinity is 34 psu, and barometric pressure is 1000 mb.

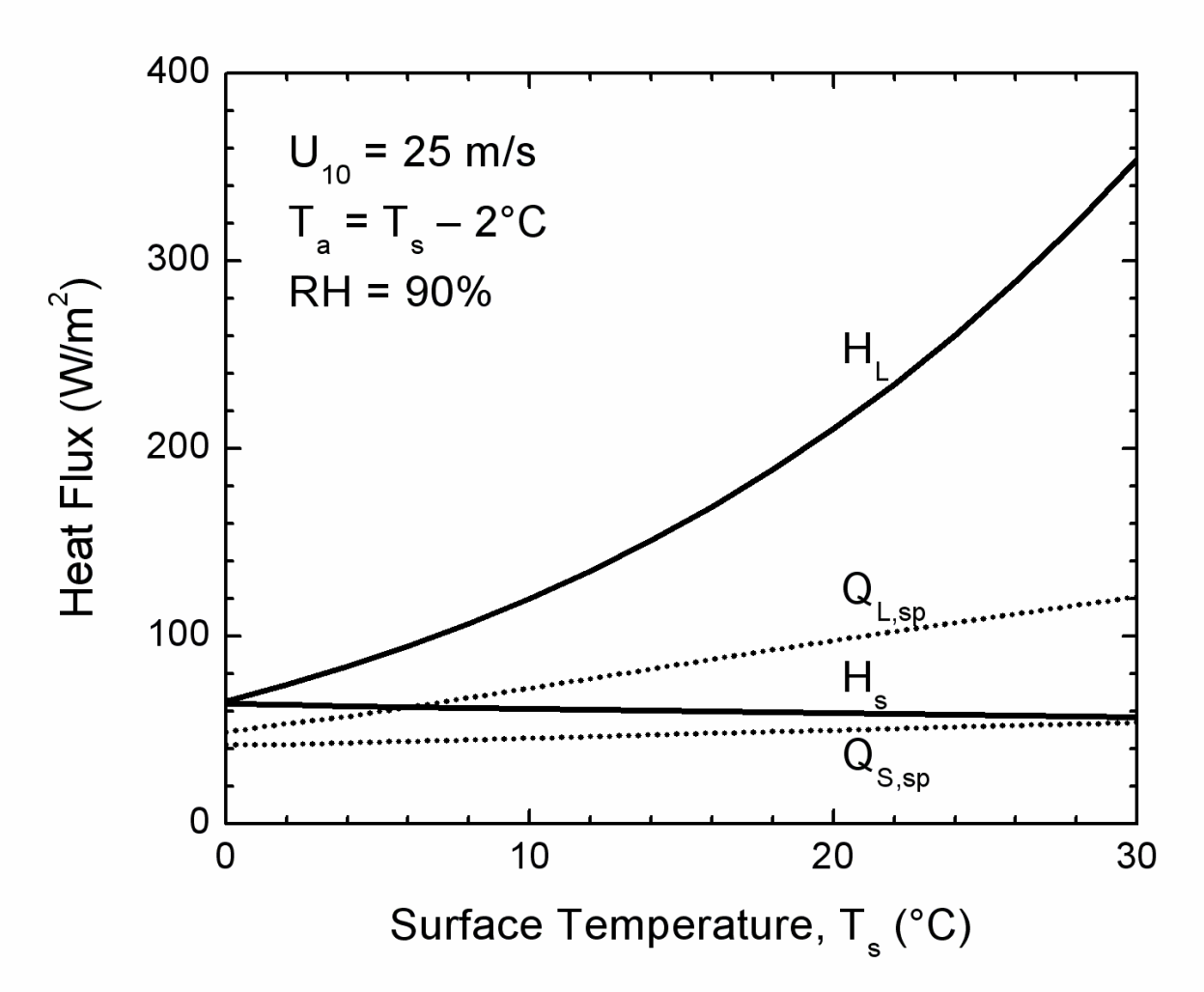

Fig. 9. As in Fig. 8, except here the fluxes are plotted against surface temperature for the wind speed fixed at 25 m s^{-1}. Again, the relative humidity is 90%, but the air temperature is always 2°C less than the surface temperature.

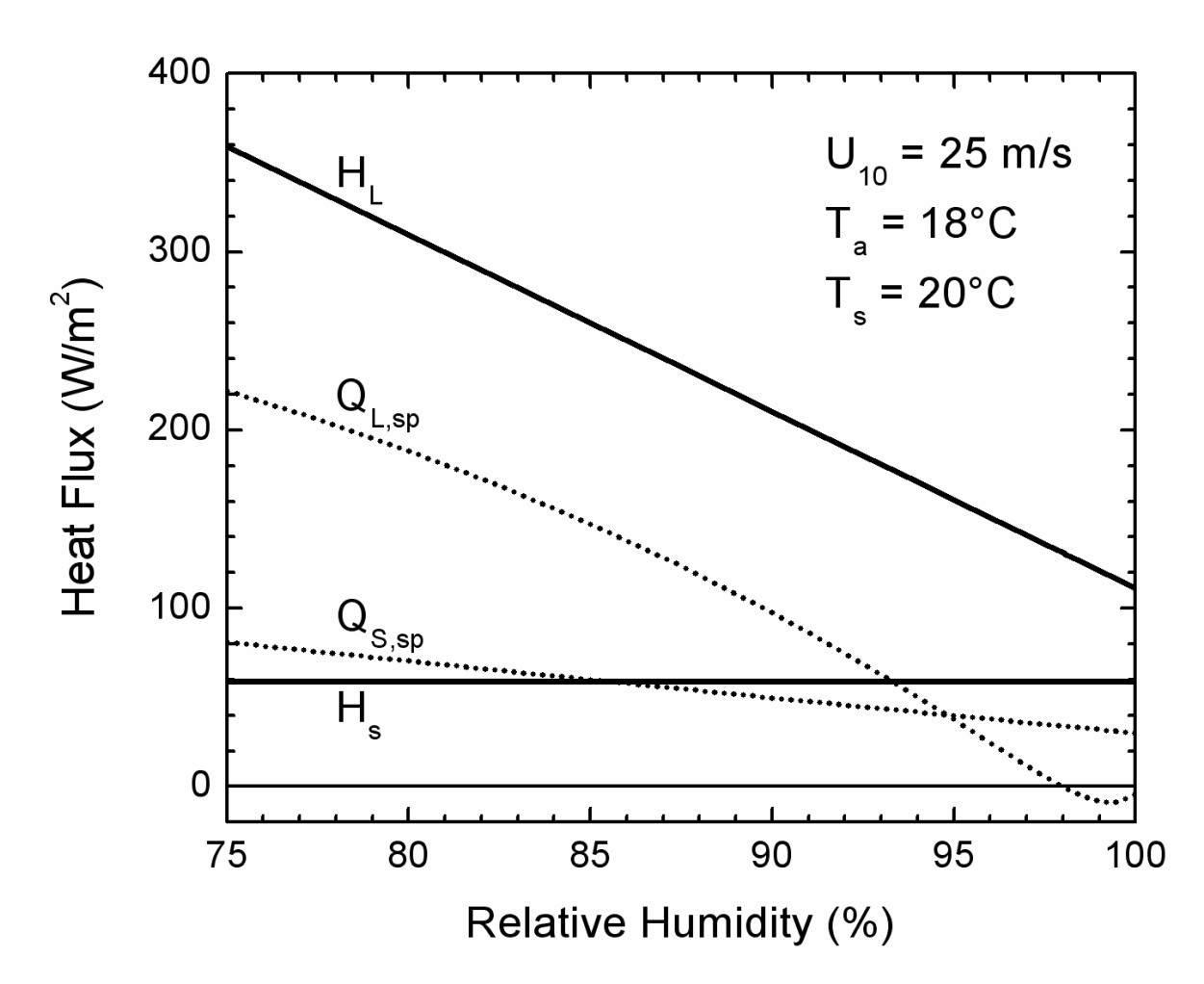

Fig. 10. As in Fig. 8, except here the fluxes are plotted against relative humidity for the wind speed fixed at 25 m s^{-1}.